



40 35p

UCRL-JC-118928
PREPRINT

Observations of Regional Phase Propagation Across the Tibetan Plateau

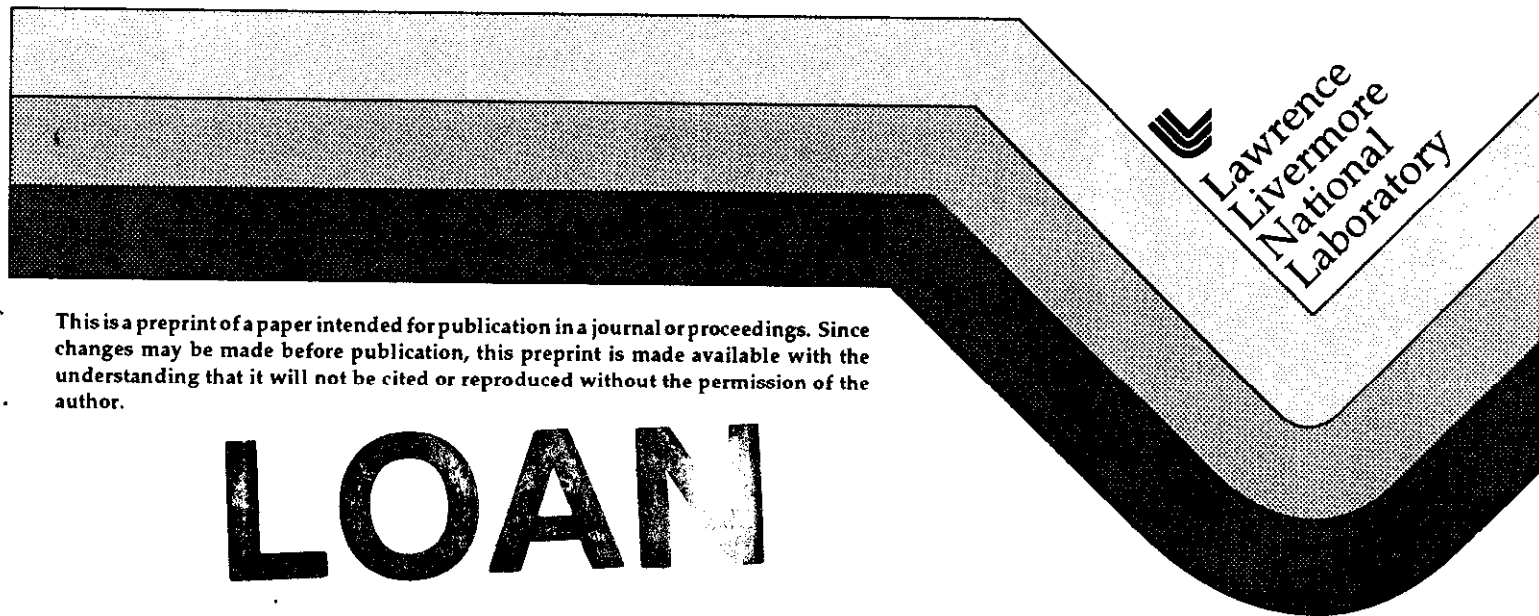
D.E. McNamara
T.J. Owens
W.R. Walter

68841 2025

CIRCULATION COPY
SUBJECT TO RECALL
IN TWO WEEKS

This paper was prepared for submittal to the
Journal of Geophysical Research

October 1994



This is a preprint of a paper intended for publication in a journal or proceedings. Since changes may be made before publication, this preprint is made available with the understanding that it will not be cited or reproduced without the permission of the author.

LOAN COPY

Observations of Regional Phase Propagation Across the Tibetan Plateau

D.E. McNamara†, T.J. Owens† and W.R. Walter‡,

† Department of Geological Sciences, University of South Carolina, Columbia, SC

‡ Earth Sciences Department, Lawrence Livermore National Laboratory, Livermore, CA

Abstract

We present observations of regional phase velocity and propagation characteristics using data recorded during a one year deployment of broadband digital seismic stations across the central Tibetan Plateau along the Qinghai-Tibet highway from Golmud to Lhasa. Previous studies of regional Tibetan Plateau earthquakes have had to rely on data recorded almost exclusively at stations outside of the plateau. We have the opportunity to study numerous source-receiver paths confined entirely within the Tibetan Plateau. Our analysis concentrates on travel-time measurements using this data set. Pn can be clearly picked for all observed paths and propagates at an average velocity of 8.1 ± 0.14 km/s across the Tibetan Plateau. Sn shows dramatic variations in propagation efficiency and, as previously reported, rapidly decreases in amplitude as it passes through the northern portion of the plateau. Additional events, from outside of the plateau, are included to map the boundaries of the region of inefficient Sn propagation. The most significant observation from this unique data set is that the entire northern portion of the Tibetan Plateau attenuates Sn energy. When observable, Sn propagates at an average velocity of 4.59 ± 0.14 km/sec across the plateau. Our results add constraints to the velocity structure of the lithosphere beneath the Tibetan Plateau.

Introduction

This paper summarizes observations of seismic velocity and propagation characteristics for high frequency, regional phases (Pg, Pn and Sn) recorded at eleven 3-component, broadband, digital seismic stations across the central Tibetan Plateau (Figure 1 and Table 1). The primary goals of this study are to determine phase velocities for Pg, Pn and Sn and also to map the lateral variation in propagation

characteristics of Sn within the Tibetan Plateau. The propagation and attenuation characteristics of Lg will be addressed in a separate study. During one year of recording (July 1991-July 1992) 183 events, at regional distances to our array, were recorded. 53 of these events were located within the Tibetan Plateau (Figure 1 and Table 2) offering a unique opportunity to observe seismic phases that both originated and were recorded entirely within the Tibetan Plateau. Previous studies of regional Tibetan Plateau earthquakes have placed first-order constraints on upper mantle velocities, but have had to rely on data recorded almost exclusively at stations outside of the plateau. Regional phase velocity and propagation characteristics are essential to obtain accurate velocity information about the crust and upper mantle. Such information is critical to understanding the tectonic evolution of this important region.

Geologic history and previous investigations. The Tibetan Plateau has intrigued geoscientists for both its impressive physiographic features as well as the relative lack of data available for interpretation. The Tibetan Plateau is comprised of a series of tectonic terranes that accreted onto the southern margin of Eurasia after the breakup of Gondwana. Since the collision of India, about 40 my ago, nearly 2000 km of convergence has occurred giving rise to the Himalaya and Karakoram ranges as well as the Tibetan Plateau (Harrison et al., 1992). The Tibetan Plateau stands out because of its high, uniform elevation and its anomalously thick crust (65-70km) (Molnar, 1988). To date, the paucity of interpretable data has not allowed for the determination of the exact tectonic mechanism that produced the Tibetan Plateau. This has led to a wide variety of tectonic evolution models, most of which fall into two basic end-member theories. First, crustal thickening and lithospheric shortening occurring in response to compression generated from continental collision between the Indian and Eurasian plates (Dewey and Burke, 1973). Second, uplift occurring by shallow underthrusting of the Indian lithosphere beneath Eurasia during collision (Argand, 1924; Barazangi and Ni, 1982; Beghoul et al., 1993).

Many first order geological and geophysical observations have been made (for review see Molnar (1988)) but information about the mantle velocity structure remains ambiguous. Previous studies, using regional phases, have been conducted with stations outside the plateau, with the exception of the Lhasa station. There are a wide range of Pn velocities reported from earlier studies. The lowest average Pn velocity reported for the Tibetan Plateau is 7.93 ± 0.17 km/s (Zhao and Xia, 1993). Other estimates

report Pn and Sn velocities of 8.1 km/s and 4.7 km/s respectively (Chen and Molnar, 1981; Jia et al., 1981; Ding et al., 1993). Still other studies have found significantly higher velocities for Pn and Sn (8.43 km/s, 4.73 km/s) (Barazangi and Ni, 1982; Ni and Barazangi, 1983; Beghoul et al., 1993). The results of the separate studies led their authors to favor opposing theories for the evolution of the Tibetan Plateau.

Data

The data used in this study were digitally recorded using broadband Streckeisen STS-2 sensors at 11 sites within the central portion of the Tibetan Plateau (Owens et al., 1993b). Initial event locations were determined from the U. S. Geological Survey (USGS) monthly Preliminary Determination of Epicenters (PDE) catalog. Locations for a small subset of Tibetan Plateau events have been improved and will be discussed later. We have examined local and regional events to determine the propagation velocities and characteristics of the phases Pg, Pn and Sn. For seismic phase velocity calculations, we have restricted our analysis to paths entirely within the plateau. This includes 53 events with epicenters within the Tibetan Plateau (Figure 1 and Table 2). We define the boundaries of the Tibetan Plateau as the 4000 m elevation contour (Figure 1). An additional 130 regional events, with sources located outside of the plateau, were recorded and are used to evaluate the propagation characteristics of Sn (Table 3).

The phase, Pg, as used in our study is the direct compressional arrival that propagates at local distances within the crust. Previous authors have shown that Pg is the first arrival for epicentral distances less than approximately 333 km (3°) within the Tibetan Plateau. Beyond this distance Pg is observed as the second major arrival, behind the much smaller amplitude Pn. The regional crossover distance can be seen as a change in slope in the first arrival travel times versus distances plotted in Figure 2a. Both Pn and Sn are regional distance refracted or turning waves that travel directly beneath the Moho in the high velocity upper-mantle lid. Velocity variations of Pn and Sn can be used to determine regional variations within the upper mantle beneath the Tibetan Plateau.

DISCLAIMER

This document was prepared as an account of work sponsored by an agency of the United States Government. Neither the United States Government nor the University of California nor any of their employees, makes any warranty, express or implied, or assumes any legal liability or responsibility for the accuracy, completeness, or usefulness of any information, apparatus, product, or process disclosed, or represents that its use would not infringe privately owned rights. Reference herein to any specific commercial product, process, or service by trade name, trademark, manufacturer, or otherwise, does not necessarily constitute or imply its endorsement, recommendation, or favoring by the United States Government or the University of California. The views and opinions of authors expressed herein do not necessarily state or reflect those of the United States Government or the University of California, and shall not be used for advertising or product endorsement purposes.

Observed Phase Velocities Within the Tibetan Plateau

Pn observations. Pn was manually picked as the first motion on the vertical component at regional distances to our array. To aid in picking, we examined broadband, high pass filtered (corner 1 Hz) and band pass filtered (corner 0.5-4 Hz) records as well as the envelopes of each passband. Pn arrival time was chosen as the earliest clear arrival of all passbands examined. Some examples of Pn can be seen in the event record sections used to illustrate Sn behavior. Because both multiple stations and multiple events were used, travel times were corrected for both focal depth and station elevation. This was done by computing a travel time correction by simply multiplying the vertical slowness by the deviation in station elevation or focal depth from the reference datum at sea level. The result of these corrections was a slight reduction of travel time data scatter.

Figure 2a shows 1090 corrected, first arrival picks from 183 events recorded at regional distances to our array. Pn is the first arrival and can be fit by a straight line between the regional crossover distance at approximately 270 km out to about 1800 km where deep turning P waves arrive before Pn. A velocity of 8.29 ± 0.18 km/sec with an intercept time of 13.5 s was obtained by fitting travel times in the distance range where Pn is the first arrival on the seismogram. The Pn-Pg crossover distance of 270 km apparent in Figure 2a is less than the approximately 333 km (3°) crossover distance observed in previous studies with less pure path plateau data, but we will still use 333 km as a minimum distance in our Pn velocity calculations to avoid contamination by Pg arrivals near the crossover distance. It is apparent from Figure 2a that the slope of the Pn arrival trend decreases with increasing distance beyond about 1500km, indicating that there is a positive velocity gradient in the upper mantle. Previous studies have provided additional evidence for an upper mantle velocity gradient (Holt and Wallace, 1990; Zhao and Xie, 1993). In addition, our data shows a sharp change in slope of initial arrival times around 1800km. This is due to deep turning P-waves in the mantle transition zone (about 400km depth). In order to focus our study on the uppermost mantle beneath the plateau, we will restrict our analysis to paths that are both entirely confined within the plateau and between distances of 333-1777 km ($3-16^\circ$).

When we restrict our observations to paths entirely within the plateau, 263 Pn first arrivals were obtained from the 53 events within the plateau. Travel time picks are shown in Figure 2b and were fit

between the distances of 333-1777 km (3° - 16°). This tighter distance range is used to eliminate any contamination from slower Pg phases near the crossover distance (270 km) and faster deep mantle P waves arriving first around 1800 km. A velocity of 8.1 ± 0.14 km/sec was obtained from the slope of the L2 fit, with an intercept of 12.7 sec. The Pn velocity obtained from paths restricted to the plateau is lower than that obtained from the entire regional data set, as well as lower than estimates obtained by including paths longer than 1800 km. The intercept time and Pn velocity corresponds to a crustal thickness of approximately 60 km when a crustal velocity of 6.1 km/s is assumed. This is comparable to previously published thickness estimations (Molnar, 1988). Uncertainty is relatively high due to scatter of the travel times (Figure 2c).

Figure 2c shows residuals from the L2 fit of Pn. Some are nearly 10 sec while most are at least 1-5 sec. Such wide scatter is indicative of either poor picks, inaccurate event locations or laterally heterogeneous velocity structure in the lithosphere beneath the Tibetan Plateau. While Pn is often emergent and difficult to precisely pick, in most cases a precision of at least 0.5 sec was obtainable. For this reason we considered larger residuals to be related to structure and/or event location errors. In a later section, we describe attempts to reduce residuals through improving event locations.

Sn observations. When we restrict our analysis to paths within the Tibetan Plateau, Sn arrivals are rare. As observed by Ni and Barazangi (1983) and Barazangi and Ni (1982), Sn energy is attenuated for paths that cross the north-central portion of the plateau. We were able to pick only 36 clear Sn arrivals from our data set of Tibetan Plateau events. An Sn velocity of 4.59 ± 0.14 km/sec was obtained by an L2 fit to these observations. This is a typical velocity for continental Sn paths. Most residuals fall within 5 seconds of the mean and all within 10 seconds. Uncertainty is large due to the lack of Sn observations and our computed Sn velocity is lower than those in previous reports (Molnar, 1988).

Pg observations. Pg was fit for two distance ranges since it is unclear at what distance the exact regional crossover occurs. If we use the previously observed crossover distance and fit all initial arrivals less than 333 km (3°) an L2 fit computed a Pg velocity of 6.73 ± 0.36 km/sec for 90 observations. When the distance range is decreased to 0-270 km Pg velocity decreases to 6.14 ± 0.23 km/sec. The first, velocity estimate is exceptionally high and may be a function of the ambiguity in the exact crossover dis-

tance. This indicates that the crossover distance is less than the previous estimate of 333km (3°). Contamination by faster Pn arrivals beyond the actual crossover distance and error mapped into travel time picks, due to mislocation of events, will affect the velocity estimate. At smaller distances, event depth and location errors cause relatively larger residuals than at greater distances. For these reasons, an exact crossover distance is difficult to determine. To be consistent with an intercept of 12.7 sec the crossover should occur around 320 km if we assume a crustal velocity of 6.1 km/s and a crustal thickness of 60 km. Though scatter is high at the crossover distance it appears that it is less than 320 km (Figure 2). The discrepancy between the intercept time and the crossover distance is likely due to errors in event location with the plateau, as discussed in the next section.

Event Relocation

Event locations and focal depths reported by the USGS PDE catalogs have been shown to be in error by as much as 25 km within the Tibetan Plateau (Zhao and Helmberger, 1991). Global earthquake locations are generally obtained by assuming an average crustal thickness of 30 km crust. However, the Tibetan Plateau crust is anomalously thick (60-75 km), so this assumption breaks down. Consequently earthquake locations reported within the Tibetan Plateau are likely in error. To investigate the size and impact of these errors on our estimates of Pn velocity, we have attempted to improve the locations of 16 local and regional earthquakes within the Tibetan Plateau. Mislocations can lead to large residuals in travel time curves, inaccurate fits and consequently inaccurate measurements of mantle velocity and crustal thickness.

To explore the effects of epicenter mislocation on our estimates of Pn velocity, we tried a simple grid search procedure to determine a new event epicenter and Pn velocity that best reduces the travel time residuals. The event epicenter is moved in a 1° by 1° grid, in 0.01° increments, centered about the initial PDE location. At each new latitude/longitude grid point, travel times are plotted versus the new epicentral distance to each recording station and a new line is fit. Both L2 and the L1 fitting techniques are used. The grid point that produces the lowest standard deviation from the L2 fit and the lowest smallest mean error from the L1 fit is considered the new event location. Both origin time and focal

depth are fixed in the relocation procedure because they will not have an effect on Pn velocity, only on the intercept time. Since we are interested in Pn velocity and event location obtained by minimizing residuals, the intercept time is not used. Adjustments to travel times for origin time and focal depth corrections at each location would not help reduce individual station residuals since Pn velocity remains unchanged. By fixing both origin time and focal depth and thereby travel time, and only varying event location, we are analyzing relative travel times between recording stations. Finally, since we are fitting travel times across the plateau we are assuming only that a one dimensional velocity structure is adequate and picking errors are small. No specific velocity structure is assumed. This technique allows us to explore the effects of event mislocation on the Pn velocity without the circularity of having to assume a particular velocity model.

From the 16 well-constrained new locations, we obtained an average relocation distance of 15.06 km. Relocation values ranged from just a few kilometers to as much as 34 km. Individual event measurements of Pn velocity using the improved locations vary considerably (7.9-8.4 km/s). The large range of individual event Pn velocity estimates is a indication of lateral heterogeneity across the Plateau. Pn velocity from an individual event is biased by the individual event station paths because of the small number of observations. Accurate determination of an average Pn velocity requires a large number of observations. Individual paths may be useful to characterize local variations in velocity structure.

Since travel time is fixed in our relocation procedure, the individual event intercept times are not used in the relocations. Travel times were normalized to an intercept time of zero by removing individual event intercept time measurements. Shown are 122 normalized travel times plotted versus the distances obtained from the 16 improved event locations as well as the 16 original, PDE, locations (Figure 3a). When compared to the travel times for the original locations (Figure 3a) it is apparent that the average Pn velocity changes only slightly when locations are improved. This suggests that average Pn velocity is insensitive to event mislocations. Errors are averaged out when a large number of travel time observations are used. These results suggest that a Pn velocity in the range of 8.1 km/s is a good average for the Tibetan Plateau and that a large number of arrivals should be used in the determination. Figure 3b shows that despite relocation, scatter is not significantly reduced overall. Since we have elim-

inated event location errors as a source of scatter, it is reasonable to conclude that the scatter in Figures 2 and 3 is due to lateral variations in seismic velocity within the Tibetan Plateau.

Regional Phase Propagation Characteristics

Sn propagation across the Tibetan Plateau. The later regional phase, Sn, shows interesting propagation variations across the Tibetan Plateau. We have divided our analysis of Sn propagation into two parts based on location of the epicenter. First, we analyze event/station paths restricted to the Tibetan Plateau (Table 2). Our experiment is unique in that this is the first time such data has been available. This data set removes any effect of the plateau boundaries on Sn amplitude and allows for detailed mapping of propagation characteristics. Second, we analyze events with locations outside of the Tibetan Plateau (Table 3). This second data set enables us to determine any effect that the plateau boundaries may have on the propagation characteristics of the Sn phase. By combining information from these two data sets, we can resolve ambiguities from previous studies that have not had access to multiple recording stations on the Tibetan Plateau.

Our analysis procedure was simplistic in that we merely noted if Sn was present, absent or weak on the band pass (1-5 Hz) seismogram at the time appropriate for waves traveling at our measured Sn velocity of approximately 4.6 km/s. We examined individual event high frequency record sections in both the radial and tangential components of motion for the presence of Sn. After this determination, we mapped the event/station paths to determine the spatial pattern of Sn propagation.

165 paths from 53 Tibetan Plateau events are shown in Figure 4a and b. Figure 4a shows paths where Sn energy is clearly observed on both the radial and tangential components of motion. Figure 4b indicates paths where no significant Sn energy is observed. A greater number of paths do not have Sn energy observable on the seismogram. It is clear that Sn does not propagate efficiently across the central Tibetan Plateau suggesting that our results are in agreement with a zone of inefficient Sn propagation proposed by Barazangi and Ni (1982). However, the density of our observations enable us to more precisely define the boundaries of this poor-Sn zone. Specifically, we suggest that the entire northern portion of the plateau effectively blocks the propagation of Sn.

To demonstrate the variable nature of Sn propagation across the Tibetan Plateau, record sections of several events are shown in Figures 5-10. Event-station paths, for these events, are shown in Figure 11a. The record sections are plotted with a Pn reducing velocity of 8.1 km/sec and Sn travel time predictions are included for reference. Both the radial and tangential components of motion are shown, band pass filtered (1-5 Hz) to suppress the large amplitudes of the surface waves and to simulate a short period instrument. The seismograms are each scaled to peak amplitude for comparison of the traces, eliminating any distance dependent amplitude variations.

Event 91.222.20.21.24 (Figure 5) occurred within the region of inefficient Sn propagation proposed by Ni and Barazangi (1983) and shows no significant Sn energy. Sn is either not generated, or severely attenuated. Event 92.095.17.42.50 (Figure 6) in Southern Tibet (Figure 11a), shows Sn propagating to SANG, AMDO, USHU, GANZ and WNDO and weak to nonexistent at MAQI, ERDO, BUDO and TUNL. Note the decrease of Sn energy at WNDO relative to AMDO. This suggests that the southern boundary of the zone of inefficient Sn propagation is transitional and allows some Sn energy to enter. However, the energy quickly dies out as evidenced by the complete lack of Sn at ERDO and BUDO. A second interesting effect is the dramatic energy decrease along the same azimuth from USHU to MAQI. This suggests a significant change in upper mantle properties between the two stations that can be explained by extending the poor Sn zone eastward. Also this indicates that radiation pattern is not the cause for the absence of Sn at MAQI for this event.

Additional support for the eastward extension of the zone of inefficient propagation can be seen with event 91.242.14.30.58 (Figures 7 and 11a). At distances less than 300 km crustal shear energy is present on the seismograms (USHU, MAQI) however, beyond 300 km Sn is nonexistent. This would suggest that event 91.242.14.30.58 (Figure 7) is being effected in a manner similar to event 91.222.20.21.24 (Figure 5) and that this event is likely within a zone in which Sn energy is not generated or quickly attenuated (Figure 11a). The western boundary can also be verified and mapped in more detail with our data set. For example, note the complete absence of Sn in event 92.096.07.47.27 (Figure 8) from the western Tibetan Plateau. The fact that station GANZ, SANG and LHSA have no apparent Sn indicates that the zone of inefficient Sn propagation may extend farther to the west than

previously suggested.

Sn propagation from outside the Tibetan Plateau. We have included additional events, with source locations outside of the plateau to add further constraints to the spatial distribution of Sn propagation. The most significant observation from this data set is that the southern boundary of the Tibetan Plateau has little to no effect on the propagation of Sn. Event 91.341.13.57.39, from directly south of the plateau (Figures 9 and 11a) demonstrates that the Himalaya mountain range does not adversely affect Sn propagation. Sn clearly arrives at all stations in the southern portion of the array but is absent from stations to the north. Again a rapid energy decrease occurs as Sn propagates from WNDO to ERDO and from USHU to MAQI. The same propagation characteristics are observed for event 92.095.17.42.50 (Figure 6) and can be used to add constraints to the southern and eastern boundaries of inefficient Sn propagation.

Event 92.024.05.06.18, from the west in Pakistan (Figures 10 and 11a), can be used in conjunction with event 92.096.07.47.27 (Figure 8) to help better define the western boundary of Sn attenuation. Note the strong Sn arrival at XIGA and its absence at AMDO (Figure 10). This observation provides evidence for the western boundary of the zone of poor Sn propagation. It cannot extend past the path from event 91.024.05.06.18 to the station XIGA (Figure 11a). It appears that S energy crosses through the north-central plateau since an arrival is apparent at the station USHU. This is likely not Sn since the epicentral distance is beyond 1800 km. Instead this is shear energy that travels deeper in the mantle than Sn and apparently propagates more efficiently beneath the north-central portion of the plateau. This would suggest that the mechanism effecting the propagation of Sn is contained within the upper portion of the mantle.

Due to our station coverage, we are not able to add constraints to the northern boundary of the Sn attenuation zone. We support the idea that it is likely coincident with the Kunlun front as previously suggested by Ni and Barazangi (1983) (Figure 11). The remaining three boundaries can be redrawn based on our new observations as shown in Figure 11a and b. Our data suggests that the entire northern portion of the Tibetan Plateau attenuates Sn rather than just the smaller zone in the north-central portion of the plateau as previously suggested by Ni and Barazangi (1983).

Discussion

Upper mantle structure beneath the Tibetan Plateau. Regional Pn and Sn velocities are commonly used to determine the nature of the uppermost mantle. These velocities vary greatly between stable shield regions and those that are tectonically active. For example, Pn and Sn propagate with velocities of 8.4 and 4.5 km/s respectively, beneath the Indian Shield (Ni and Barazangi, 1983). Relatively lower Pn and Sn velocities are typical of regions of high heat flow and active tectonics. Pn velocity measured in the tectonically active Basin and Range Province is as low as 7.8 km/s and Sn has been shown not to propagate (Beghoul et al., 1993; Benz et al., 1990). Based on this information Pn and Sn have been used to attempt to distinguish between the two basic theories describing the mechanism of uplift of the Tibetan Plateau. If India has underthrust the Tibetan Plateau, then the mantle beneath the plateau should closely resemble the structure beneath the Indian Shield. Our Pn and Sn velocities beneath the plateau, fall within the middle of the velocities expected for the two end member models. Molnar (1988) argued that an increase in pressure within the upper mantle of the Tibetan Plateau due to an anomalously thick overlying crust could increase the Pn velocity by as much as 0.15 km/s. If this correction were applied to our Pn velocity, it would decrease to less than 8.0 km/s. This is a value more typical of a tectonically active region and well below a Pn velocity expected if the Indian Shield is underthrust beneath the Tibetan Plateau. An additional correction could be applied to our Pn velocity to correct for a velocity gradient in the mantle-lid. The effect of correcting for a positive gradient would also result in the reduction of the average Pn velocity (Zhao and Xie, 1993).

The north-central Tibetan Plateau is particularly interesting because of the large amount of seismic data that can be interpreted as evidence for high temperatures in the upper mantle. For example, previous studies have reported observations of large teleseismic S-P travel time residuals (Molnar and Chen, 1984; Molnar, 1990), slow Rayleigh phase velocities (Brandon and Romanowicz, 1986), and large values of shear wave splitting (McNamara et al., 1994). Each observation, in addition to the inefficient Sn propagation, is in support of anomalous heat production in the northern portion of the plateau. The seismic evidence is also supported by surface geologic observations. In the northern Tibetan Plateau there is strong evidence for widespread Cenozoic volcanism with both basaltic and granitic

components (Deng, 1978; Dewey et al., 1988; Molnar, 1988). The basaltic composition suggests volcanic sources are from partial melt of upper mantle material.

The region of inefficient Sn propagation reported here expands the zone previously reported by Ni and Barazangi (1983) since we have more accurately defined its boundaries with our numerous additional propagation paths. More specifically, we suggest that the poor Sn zone be extended to include the entire northern portion of the Tibetan Plateau (Figure 11b). Previous studies have shown that Pn velocity in the northern plateau is slow relative to the south (Holt and Wallace, 1990; Zhao and Xie, 1993). Low Pn velocity coincident with the zone of Sn attenuation would not be surprising and we plan to add further constraints to this idea with Pn tomography using our pure-path data set. We have observed large residuals within our Pn travel time data set despite relocations of Tibetan Plateau events. We expect that the remaining residuals are likely do to lateral heterogeneity within the mantle-lid of the plateau.

Conclusions

We have developed improved constraints on regional seismic wave propagation within the Tibetan Plateau. The new areal and distance coverage provided by our temporary deployment allows us to analyze a large number of propagation paths confined to the plateau interior for the first time. Using these data, we have determined an average Pn velocity for the plateau of 8.1 ± 0.14 km/s. This velocity appears somewhat higher than other tectonically active regions, but is in the lower range of Tibetan Plateau Pn velocities. If pressure and velocity gradient corrections were applied, the Pn velocity would be comparable to tectonically active areas with normal crustal thickness. By utilizing a restricted distance range and paths confined entirely to the plateau, we have determined an average Pn velocity appropriate for the uppermost mantle beneath the interior of the plateau. Despite the path restrictions and attempts to improve event locations, the scatter of Pn travel times remains large, indicating velocity heterogeneity within the plateau. Further characterization of this heterogeneity may be possible through tomographic analysis of our Pn travel-times as well as waveform modeling of individual station-event paths.

The Sn velocity estimate determined in this study is also high relative to other tectonically active regions, but is biased by the lack of measurable Sn arrivals. The Sn phase is severely attenuated throughout the entire northern plateau, extending a zone of inefficient Sn propagation previously identified in the north-central plateau (Barazangi and Ni, 1982; Ni and Barazangi, 1983). Observations of crustal shear waves and shear waves at greater distances propagating through this zone suggests that the mechanism impeding Sn propagation is confined to the uppermost mantle within the northern plateau.

Acknowledgments

The authors would like to thank the many scientists and field workers who endured the hardships of the Tibetan Plateau and greatly contributed to the success of this experiment. Contributors included Chinese participants from the Institute of Geophysics, State Seismological Bureau, PRC and the Seismological Bureaus of the Qinghai Province and the Tibetan Autonomous Region. U.S. participants in the field program included R. Busby (PIC-LDGO), R. Kuenel (Carnegie-DTM), G. Randall, G. Wagner, S. Owens and M. Salvador (USC). This project was supported by NSF grants EAR-9004428, EAR-9196115 and EAR-9206815 to USC. Event relocation work was supported by LLNL in the summer of 1993, and performed under the auspices of the U.S. Department of Energy by Lawrence Livermore National Laboratory under contract W-7405-ENG-48.

References

- Argand, E., La tectonique de L'Asie, *Proc. 13th Geol. Cong. Brussels, 13*, 170-372, 1924.
- Barazangi, M., and J. Ni, Velocities and propagation characteristics of P_n and Sn beneath the Himalayan arc and Tibetan Plateau: Possible evidence for underthrusting of Indian continental lithosphere beneath Tibet, *Geology, 10*, 179-185, 1982.
- Beghoul, N., M. Barazangi, and B. L. Isacks, Lithospheric structure of Tibet and western North America: mechanisms of uplift and a comparative study, *J. Geophys. Res.*, 98, 1997-2016, 1993.
- Benz, H. M., R. B. Smith, and W. D. Mooney, Crustal structure of the Northwest Basin and Range pro-

- vince from the 1986 program for array seismic studies of the continental lithosphere seismic experiment, *J. Geophys. Res.*, 95, 21,823–21,842, 1990.
- Brandon, C., and A. Romanowicz, A "NO-LID" zone in the central Chang-Thang platform of Tibet: Evidence from pure path phase velocity measurements of long-period Rayleigh waves, *J. Geophys. Res.*, 91, 6547–6564, 1986.
- Chen, W. P., and P. Molnar, Constraints on seismic wave velocity structure beneath the Tibetan Plateau and their tectonic implications, *J. Geophys. Res.*, 86, 5937–5962, 1981.
- Deng, W., A preliminary study on the petrology and petrochemistry of the Quaternary volcanic rocks of the Northern Tibet Autonomous region, *Acta. Geol. Sin. Eng. Ed.*, 52, 148–152, 1978.
- Dewey, J. F., and K. C. A. Burke, Tibetan Variscan, and Precambrian basement reactivation: products of continental collision, *J. Geol.*, 81, 683–692, 1973.
- Dewey, J. F., R. M. Shackleton, F. R. S. Chang Cheng, and S. Yiyin, The tectonic evolution of the Tibetan Plateau, *Phil. Trans. R. Soc. Lond.*, 327, 379–413, 1988.
- Ding, Zhi-feng, Rong-shen Zeng, and Francis T. Wu, The Pn wave velocities and the relief of Moho in the Tibetan Plateau, *Acta Seismologica Sinica*, 6, 317–325, 1993.
- Harrison, T. M., P. Copeland, W. S. F. Kidd, and A. Yin, Raising Tibet, *Science*, 255, 1663–1670, 1992.
- Holt, W. E., and T. C. Wallace, Crustal thickness and upper mantle velocities in the Tibetan Plateau region from the inversion of regional Pnl waveforms: evidence for a thick upper mantle lid beneath southern Tibet, *J. Geophys. Res.*, 95, 12,499–12,525, 1990.
- Jia, Su-jian, Xue-feng Cao, and Jia-quan Jia, The P wave travel times and upper mantle structure of the Tibetan Plateau, *N West. seism. J.*, 3, 27–34, 1981.
- McNamara, D. E., and W. R. Walter, Lithospheric structure of the Tibetan Plateau from relocation of local and regional earthquakes, *LLNL UCID*, in press, 1994.
- McNamara, D. E., T. J. Owens, P. G. Silver, and F. T. Wu, Shear wave anisotropy beneath the Tibetan Plateau, *J. Geophys. Res.*, 99, 13,655–13,665, 1994.
- Molnar, P., and W. P. Chen, S-P travel time residuals and lateral inhomogeneity in the mantle beneath

- Tibet and the Himalaya, *J. Geophys. Res.*, 89, 6911–6917, 1984.
- Molnar, P., A review of geophysical constraints on the deep structure of the Tibetan Plateau, the Himalaya and the Karakoram, and their tectonic implications, *Trans. R. Soc. Lond.*, A327, 33–88, 1988.
- Molnar, P., S-wave residuals from earthquakes in the Tibetan region and lateral variations in the upper mantle, *Earth Planet. Sci. Lett.*, 101, 68–77, 1990.
- Ni, J., and M. Barazangi, High frequency seismic wave propagation beneath the Indian shield, Himalayan arc, Tibetan Plateau and surrounding regions: high uppermost mantle velocities and efficient propagation beneath Tibet, *Geophys. J. R. Astr. Soc.*, 72, 665–689, 1983.
- Owens, T. J., G. E. Randall, F. T. Wu, and R. S. Zeng, PASSCAL instrument performance during the Tibetan Plateau passive seismic experiment, *Bull. Seismol. Soc. Am.*, 83, 1959–1970, 1993a.
- Owens, T. J., G. E. Randall, D. E. McNamara, and F. T. Wu, Data Report for the 1991-92 Tibetan Plateau passive-source seismic experiment, *PASSCAL Data Rep. #93-005*, 1993b.
- Zhao, Lian-She, and D. V. Helmberger, Geophysical Implications from relocations of Tibetan Earthquakes: hot lithosphere, *Geophys. Res. Lett.*, 18, 2205–2208, 1991.
- Zhao, Lian-She, and J. Xie, Lateral variations in compressional velocities beneath the Tibetan Plateau from Pn traveltimes tomography, *Geophys. J. Int.*, 115, 1070–1084, 1993.

Figure Captions

Figure 1. Tibetan Plateau experiment base map showing recording stations and the distribution of 53 Tibetan Plateau regional events recorded during the one year of deployment. Additional events, outside of the 4000m contour, are shown to demonstrate Sn propagation across the boundaries of the plateau. Regional structural trends are taken from Dewey et al. (1988). Events referenced in the text are labeled with their event identifier using the notation of Owens et al., (1993b).

Figure 2. (a) Travel time picks for 1090 first arrivals, from 183 events, at regional distances to the array. This data set includes event/station paths that cross the plateau boundaries. A reference velocity of 8.1 km/sec is shown to highlight the Pg-Pn cross over distance (~ 270 km) and the distance where Pn is no longer the first arrival (~ 1800 km). (b) Travel time picks for first arrivals from events within the Tibetan Plateau. This data set is restricted to event/station paths confined to the Tibetan Plateau. Pn velocities of 8.08 ± 0.15 km/s and 8.10 ± 0.14 km/s were computed by fitting a line to 263 Pn arrivals beyond the cross over distance using both L1 and L2 fitting techniques, respectively. (b) Arrival time residuals relative to the L1 fit of 8.1 km/sec for the pure path plateau data set.

Figure 3. Pn travel times for 16 relocated regional events within the Tibetan Plateau. (a) Travel time data and velocity fits before relocation. Pn velocities of 8.14 ± 0.15 km/s and 8.08 ± 0.18 km/s were computed using both L1 and L2 fitting techniques, respectively. (b) Travel time data and velocity fits after event relocation. Pn velocities of 8.18 ± 0.15 km/s and 8.11 ± 0.14 km/s were computed using both L1 and L2 fitting techniques, respectively. (c) Residuals for data before relocation. (d) Residuals for data after relocation.

Figure 4. Sn propagation characteristics across the plateau. The shaded region in the north-central plateau is a previously identified region of inefficient Sn propagation (Barazangi and Ni, 1982). (a) Map of paths where Sn is not observed. (b) Map of paths where Sn is observed.

Figure 5. Central plateau local event record sections (91.222.20.21.24). Both the radial and tangential components of motion are shown band pass filtered (1-5 Hz) to simulate a short period instru-

ment. Dashed lines show the predicted arrival times of Pn (8.1 km/s), Sn (4.6 km/s) and Lg (3.5 km/s).

Figure 6. Southern plateau local event record sections (92.095.17.42.50). Display parameters are the same as Figure 5.

Figure 7. Regional event record sections from east of the Tibetan Plateau (91.242.14.30.58). Display parameters are the same as Figure 5.

Figure 8. Regional event record sections from the northwestern Tibetan Plateau (92.096.07.47.27). Display parameters are the same as Figure 5 except for LHSA. Data at LHSA was recorded continuously at a slower sampling rate of 5 samples/s. Both the radial and tangential components of motion are shown high pass filtered with a corner frequency of 1 Hz.

Figure 9. Regional record sections from a Burmese event, southeast of the Tibetan Plateau (91.341.13.57.39). Display parameters are the same as Figure 5.

Figure 10. Regional event record section from Pakistan, west of the Tibetan Plateau (92.024.05.06.18). Dashed lines show the predicted arrival times of Pn, Sn and Lg.

Figure 11. (a) Examples of Sn propagation from 6 separate events. Solid lines show paths where Sn is observed. Dashed lines show paths where Sn is not observed. (b) The extended zone of inefficient Sn propagation, determined from our new data set, is shown as the shaded region in the northern plateau. Also shown are regional events used in the study (stars) and the simplified regional structure (solid lines) (after Dewey et al., 1988).

Table 1

Tibetan Plateau Seismic Experiment
(Station Locations)

Station	Latitude (°N)	Longitude (°E)	Elevation (meters)
AMDO	32.247	91.688	4712
BUDO	35.529	93.910	4660
ERDO	34.520	92.707	4623
GANZ	29.767	94.050	3150
LHSA	29.702	91.128	3700
SANG	31.024	91.700	4740
TUNL	36.199	94.815	3133
WNDO	33.448	91.904	4865
XIGA	29.234	88.851	3865
MAQI	34.478	100.249	3823
USHU	33.011	97.015	3727

Table 2. Tibetan Plateau Events

Event ID†	Origin Time YRDAYHHMMSS.t	Latitude (°N)	Longitude (°E)	Depth (Km)	Mb	#stations
91.199.13.23.31	91199132459.9	30.363	94.870	33	5.0	9
91.201.18.52.05	91201190230.6	30.326	94.838	24	4.8	9
91.204.16.50.24	91204165154.0	30.269	94.820	33	4.7	9
91.205.06.06.43	91205060644.5	30.302	94.785	33	4.8	7
91.206.01.52.18	91206015245.2	30.317	94.791	33	4.8	7
91.209.23.57.54	91209235820.2	30.329	94.793	33	4.9	8
91.210.15.47.13	91210154808.8	30.269	94.793	33	4.7	9
91.211.22.21.39	91211222205.9	30.385	94.795	33	4.8	8
91.222.20.21.24	91222202151.7	33.910	92.158	10	4.7	11
91.239.05.14.10	91239051432.3	34.249	92.161	33	3.4	9
91.242.14.30.58	91242143212.8	34.449	97.309	33	4.3	8
91.270.07.39.55	91270073955.3	34.645	98.874	33	4.7	7
91.270.11.55.24	91270115640.8	29.911	90.423	33	3.7	5
91.270.23.29.56	91270233121.4	32.444	93.354	33	4.3	8
91.323.01.03.09	91323010418.0	32.484	93.593	33	4.9	10
91.325.13.36.25	91325133742.1	33.714	90.337	33	4.3	9
91.328.07.34.25	91328073526.6	33.980	88.646	33	4.7	8
91.329.10.07.40	91329100839.0	34.017	88.832	33	4.4	9
91.330.21.15.51	91330211559.9	34.073	94.247	33	4.3	10
91.336.19.44.36	91336194536.6	32.090	94.694	46	4.4	9
91.348.08.19.24	91348082023.8	33.976	88.840	33	5.1	8
91.349.15.58.26	91349155932.8	29.970	93.928	33	4.8	9
91.351.20.26.50	91351202749.6	33.990	88.904	33	4.6	9
91.355.19.52.42	91355195245.5	27.904	88.139	57	4.9	9
91.357.01.57.23	91357015825.1	33.917	88.863	33	5.2	8
91.358.21.26.32	91358212752.1	30.003	92.544	33	4.4	6
91.365.21.13.33	91365211418.5	30.657	99.571	33	4.5	8
92.002.02.34.36	92002023537.2	33.990	88.859	33	4.8	9
92.007.16.23.40	92007162309.9	30.118	99.537	36	4.8	8
92.008.17.40.21	92008174141.5	30.137	92.449	33	4.0	5
92.023.10.25.28	92023102626.7	34.566	93.164	33	5.2	5
92.034.15.43.19	92034154422.6	34.496	93.147	10	4.7	6
92.037.03.34.31	92037033515.3	29.610	95.521	15	5.6	6
92.040.12.44.12	92040124452.7	29.627	95.646	10	5.1	6
92.040.14.36.56	92040143734.7	29.660	95.607	10	4.8	2
92.065.02.15.19	92065021417.6	35.625	80.585	36	4.7	3
92.067.22.40.50	92067224150.8	29.442	89.370	113	4.3	5
92.076.01.18.29	92076011855.9	34.343	86.288	33	4.7	6
92.084.19.32.48	92084193210.3	31.545	81.540	16	4.8	3
92.090.18.27.39	92090183006.6	31.929	94.465	33	3.9	9
92.092.20.54.29	92092205403.7	31.964	83.754	52	4.1	3
92.095.17.42.50	92095174320.7	28.147	87.979	33	4.9	9
92.096.07.47.27	92096074747.6	35.696	80.661	18	5.5	9
92.096.11.08.11	92096110923.1	35.665	80.599	33	4.0	2
92.104.03.46.58	92104034751.0	31.958	88.339	33	4.6	9
92.109.18.19.52	92109181929.2	36.155	92.538	10	4.1	9
92.119.01.36.25	92119013628.9	32.145	85.066	33	3.8	4
92.130.07.23.48	92130072344.8	34.503	84.774	10	4.6	3
92.139.19.55.16	92139195538.8	34.858	86.331	33	4.1	6
92.143.05.46.46	92143054731.5	30.748	99.685	33	4.6	6
92.173.08.07.07	92173080746.5	30.428	89.394	28	4.2	2

92.179.02.14.16	92179021318.3	35.148	81.079	33	4.5	4
92.179.13.22.17	92179132120.9	35.139	81.131	33	5.0	4

† based on the notation of Owens et al (1993b).

Table 3. Regional Events off the Tibetan Plateau

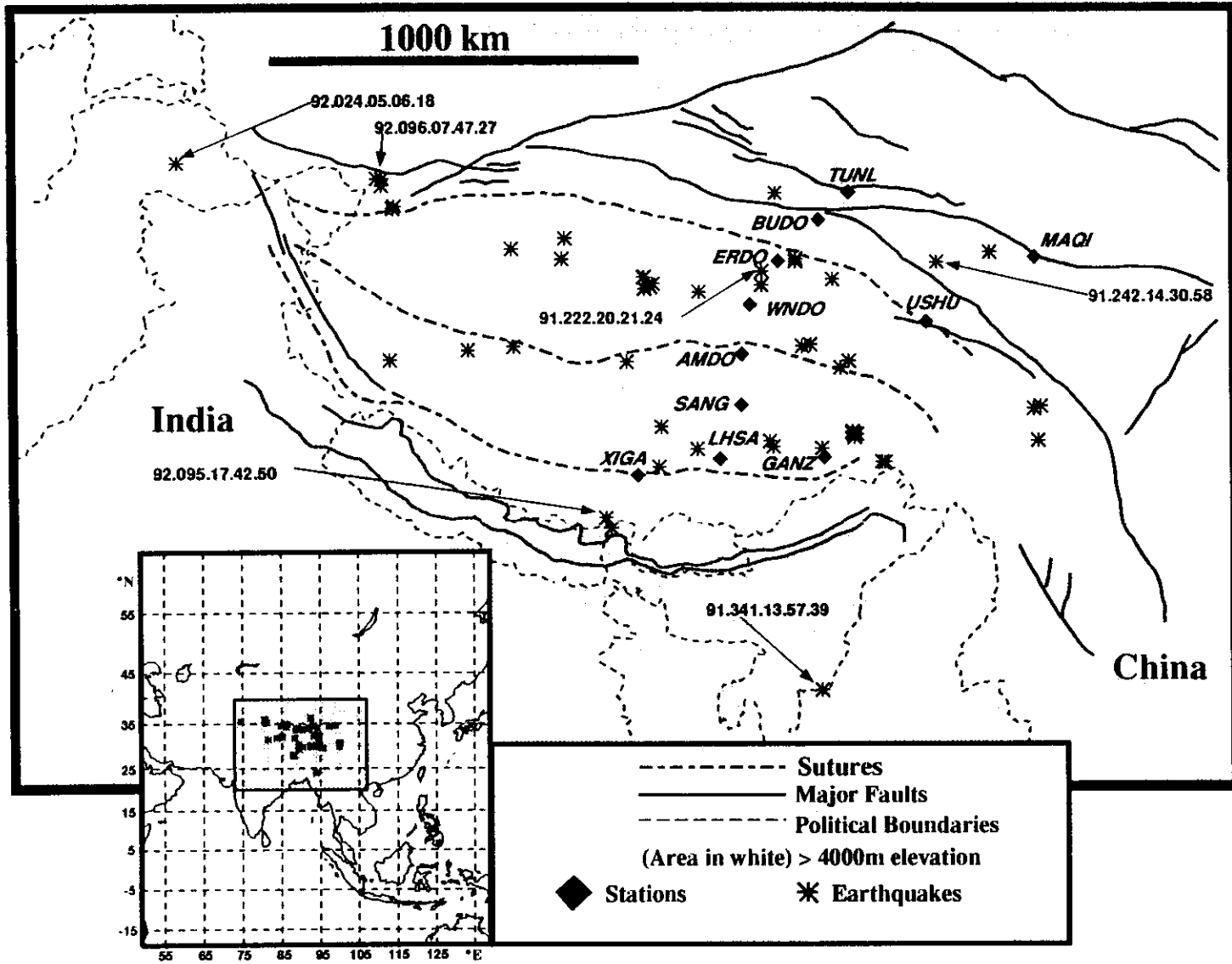
Event ID†	Origin Time YRDAYHHMMSS.t	Latitude (°N)	Longitude (°E)	Depth (Km)	Mb	#stations
91.193.21.55.49	91193220600.2	39.421	94.832	16	4.8	4
91.199.09.53.55	91199095036.7	8.224	94.112	27	5.4	5
91.199.15.27.32	91199152405.1	8.439	94.629	16	5.1	1
91.199.17.44.50	91199174543.5	30.362	94.667	33	4.2	6
91.201.18.52.00	91201185223.9	30.298	94.741	33	4.5	7
91.204.13.29.37	91204132547.3	3.775	95.932	47	5.8	8
91.210.03.18.45	91210032015.6	30.294	94.765	33	4.6	5
91.215.08.38.02	91215083317.1	29.330	129.081	17	5.5	2
91.216.12.42.55	91216123824.5	23.888	95.859	43	4.7	8
91.218.02.21.24	91218021731.6	3.827	95.374	18	6.0	6
91.220.11.15.33	91220111238.4	26.879	65.848	53	5.3	10
91.231.06.07.09	91231060551.3	46.944	85.302	30	5.5	8
91.234.03.53.11	91234035341.1	25.030	91.330	33	4.7	9
91.234.21.26.07	91234211504.5	55.771	114.364	23	5.2	1
91.235.07.39.13	91235073625.8	36.155	68.802	33	4.9	5
91.236.17.46.43	91236174523.3	38.441	75.213	33	4.7	4
91.237.05.04.30	91237050059.8	5.649	94.116	44	5.2	7
91.238.20.45.55	91238204231.8	6.937	94.531	26	5.4	9
91.238.20.54.25	91238205423.0	6.882	94.609	22	5.8	8
91.245.11.05.48	91245110550.4	37.440	95.402	10	5.5	11
91.247.08.35.12	91247083233.5	10.746	92.843	33	5.1	8
91.247.22.31.26	91247222721.7	15.204	120.404	21	5.6	3
91.250.03.00.10	91250030024.3	24.252	93.976	33	4.9	7
91.251.23.53.44	91251235441.5	36.626	98.553	23	4.8	8
91.252.21.54.32	91252215450.5	28.879	94.937	33	4.8	11
91.255.00.45.09	91255003330.7	54.905	111.112	25	5.1	3
91.255.23.05.10	91255230630.1	29.698	95.688	34	4.6	7
91.257.13.17.47	91257131639.7	40.171	105.046	25	5.1	10
91.258.00.23.59	91258002050.3	30.617	66.735	33	4.8	5
91.258.02.15.33	91258021224.9	30.724	66.763	26	4.6	5
91.260.18.53.51	91260185322.2	43.141	87.968	22	4.8	4
91.262.04.23.29	91262042356.7	26.323	92.211	33	4.7	6
91.263.09.41.20	91263093742.5	44.832	90.332	33	4.8	2
91.263.11.15.36	91263111611.5	36.191	100.063	13	5.5	10
91.265.05.45.35	91265054227.8	30.165	67.799	10	4.9	1
91.273.09.47.58	91273094442.1	22.535	121.479	24	5.5	7
91.273.16.33.41	91273163306.2	37.766	101.323	20	5.3	11
91.273.18.35.45	91273183544.2	22.728	94.416	75	4.7	10
91.274.20.33.26	91274203020.0	35.705	65.512	12	5.3	10
91.279.10.58.20	91279105044.4	21.384	104.231	10	4.5	3
91.279.12.16.45	91279121812.0	37.677	101.437	10	4.1	3
91.285.05.12.00	91285050836.3	22.798	121.536	8	5.1	3
91.285.12.23.03	91285122347.2	37.791	101.176	36	4.3	5
91.288.19.11.31	91288191100.9	30.565	79.311	33	4.5	2
91.292.21.24.47	91292212314.3	30.780	78.774	10	6.5	11
91.293.05.34.33	91293053226.8	30.790	78.686	27	4.9	2
91.296.20.41.02	91296203709.1	20.836	122.158	29	4.4	2
91.298.14.44.00	91298144039.8	23.788	122.952	27	5.2	3
91.304.02.31.18	91304022902.5	40.148	72.841	21	5.2	10
91.307.00.03.04	91307000225.9	28.365	103.984	33	4.5	2
91.312.15.16.59	91312151344.1	26.323	70.607	22	5.6	11

91.319.19.56.36	91319195343.5	29.696	69.134	19	4.6	6
91.320.12.17.40	91320121422.5	37.660	66.469	33	4.8	3
91.330.15.30.17	91330153114.7	33.919	88.746	33	4.1	8
91.337.13.19.49	91337131644.1	9.095	92.470	37	4.7	4
91.338.03.27.07	91338032724.2	24.015	93.986	72	4.9	11
91.339.15.51.42	91339154820.7	22.544	121.450	17	4.6	3
91.341.13.57.39	91341135740.6	24.059	93.913	69	5.1	11
91.341.14.26.09	91341142232.2	25.191	62.974	30	5.2	4
91.343.01.03.52	91343010246.5	29.543	81.632	29	5.6	11
91.351.23.51.10	91351234954.5	44.333	83.727	17	4.9	5
91.353.18.59.32	91353185517.4	28.102	57.304	27	5.3	3
91.354.02.05.53	91354020605.3	24.720	93.103	41	5.3	10
91.357.02.14.54	91357021454.5	33.966	88.942	33	5.0	9
91.359.12.16.26	91359121322.3	10.607	93.906	40	4.7	6
91.360.13.26.42	91360132417.7	30.837	99.532	33	4.1	5
91.361.09.11.27	91361090937.5	51.019	98.150	14	5.8	10
91.362.09.14.39	91362090703.3	51.096	98.061	17	5.0	5
92.004.03.37.35	92004033521.6	31.954	69.991	29	5.0	9
92.005.17.23.27	92005171421.0	40.873	71.172	16	5.0	2
92.005.17.30.00	92005172319.8	41.583	71.556	33	4.4	2
92.011.06.19.51	92011061655.9	9.311	86.964	22	5.7	8
92.012.00.11.55	92012001227.1	39.671	98.300	22	5.4	6
92.013.18.36.22	92013183632.1	24.439	92.557	33	4.5	5
92.020.09.01.16	92020085822.5	27.398	65.994	27	5.2	7
92.021.22.10.43	92021220758.9	26.632	67.198	26	5.4	8
92.022.21.43.49	92022214125.9	35.351	121.109	33	5.1	6
92.024.05.06.18	92024050447.3	35.515	74.529	47	5.4	6
92.025.15.16.29	92025151231.9	26.070	98.668	33	4.7	1
92.030.05.25.29	92030052201.4	24.958	63.141	29	5.5	3
92.036.11.04.57	92036105713.0	50.260	100.168	45	4.4	1
92.036.19.42.54	92036193629.8	31.513	67.038	33	4.4	1
92.036.23.13.35	92036231048.6	31.426	66.825	18	5.1	6
92.036.23.43.40	92036234136.8	31.365	66.858	33	5.0	4
92.041.12.42.34	92041123857.1	21.173	121.901	22	5.0	2
92.045.08.21.20	92045081825.7	53.897	108.866	21	5.3	3
92.054.20.07.30	92054200625.2	41.556	81.267	33	4.7	1
92.067.06.31.49	92067062855.3	40.075	71.685	25	4.9	3
92.069.17.02.51	92069165928.6	27.424	66.044	19	4.9	7
92.075.01.05.37	92075010127.1	23.548	123.562	31	5.7	8
92.077.02.17.41	92077021449.6	9.216	92.833	67	4.8	8
92.079.06.38.32	92079063425.8	17.155	120.827	15	5.7	4
92.082.01.51.00	92082014755.0	10.553	93.904	33	4.9	5
92.084.21.04.01	92084210147.5	33.832	72.905	14	5.0	9
92.085.17.19.11	92085171537.6	24.455	123.318	78	5.4	3
92.087.10.41.40	92087103930.6	35.997	72.548	35	4.9	7
92.088.10.20.59	92088101741.8	26.582	67.303	10	4.9	6
92.090.19.22.19	92090191934.8	35.855	72.374	55	4.4	1
92.092.13.40.48	92092134103.9	27.392	87.065	33	4.3	4
92.097.19.49.55	92097194911.3	44.427	101.792	33	4.7	2
92.103.18.41.18	92103183716.5	29.515	131.396	39	5.6	1
92.110.18.35.29	92110183219.0	23.861	121.594	16	5.8	1
92.111.18.49.38	92111185028.3	27.256	92.077	33	4.6	7
92.114.12.25.22	92114122117.2	29.429	131.364	40	5.8	1
92.114.14.19.00	92114141835.1	22.437	98.904	12	5.8	10

92.114.15.33.13	92114153249.1	22.418	98.852	10	5.9	10
92.114.17.20.05	92114171502.7	22.309	98.856	33	4.7	8
92.114.18.24.18	92114181811.6	22.303	98.997	33	4.8	7
92.115.07.10.45	92115070723.9	27.550	66.065	25	5.9	9
92.115.12.04.17	92115114912.3	23.768	121.660	18	4.7	2
92.119.21.08.48	92119210303.6	22.430	98.935	33	4.6	3
92.122.08.10.36	92122080945.0	19.583	94.419	55	4.6	4
92.125.10.57.33	92125105422.2	29.882	67.550	10	4.9	5
92.131.04.06.36	92131040432.9	37.207	72.913	33	5.6	9
92.132.11.21.35	92132112341.4	36.794	73.487	33	4.7	2
92.136.08.10.26	92136080802.9	41.019	72.429	50	5.7	6
92.137.08.34.31	92137083257.7	23.262	99.939	33	4.6	2
92.137.20.20.20	92137201952.9	36.080	99.869	17	5.0	8
92.141.12.22.51	92141122032.8	33.377	71.317	16	6.0	9
92.142.05.00.01	92142045957.5	41.604	88.813	00	6.5	8
92.146.05.10.38	92146050813.1	36.701	71.046	48	4.9	6
92.147.19.00.39	92147185654.8	20.100	121.396	53	4.9	1
92.154.22.08.09	92154220745.3	28.984	81.913	56	5.2	9
92.155.01.59.24	92155015513.3	28.083	128.094	56	4.9	1
92.155.02.41.37	92155024236.6	33.905	88.893	10	4.6	7
92.157.00.26.01	92157002343.7	33.241	71.228	33	4.9	6
92.162.13.41.31	92162134124.9	25.660	96.758	33	4.7	5
92.165.16.56.33	92165165507.7	39.845	77.828	35	4.7	3
92.167.02.49.28	92167024856.2	24.027	95.932	17	5.8	5
92.173.11.11.02	92173111939.7	38.307	99.423	20	4.8	3

† based on the notation of Owens et al (1993b).

(Figure 1: McNamara et al., 1994)



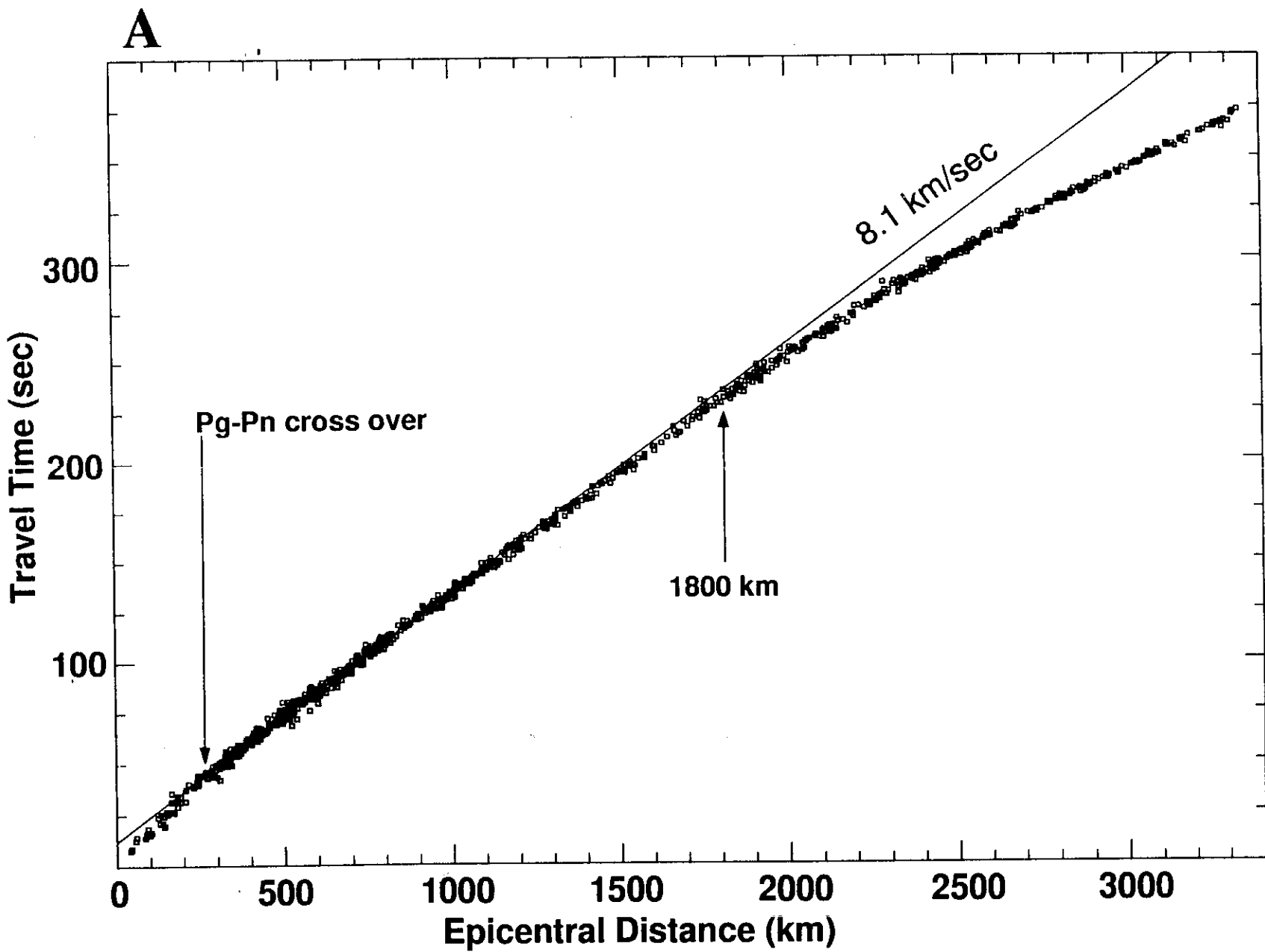


(Figure 2: McNamara et al., 1994)

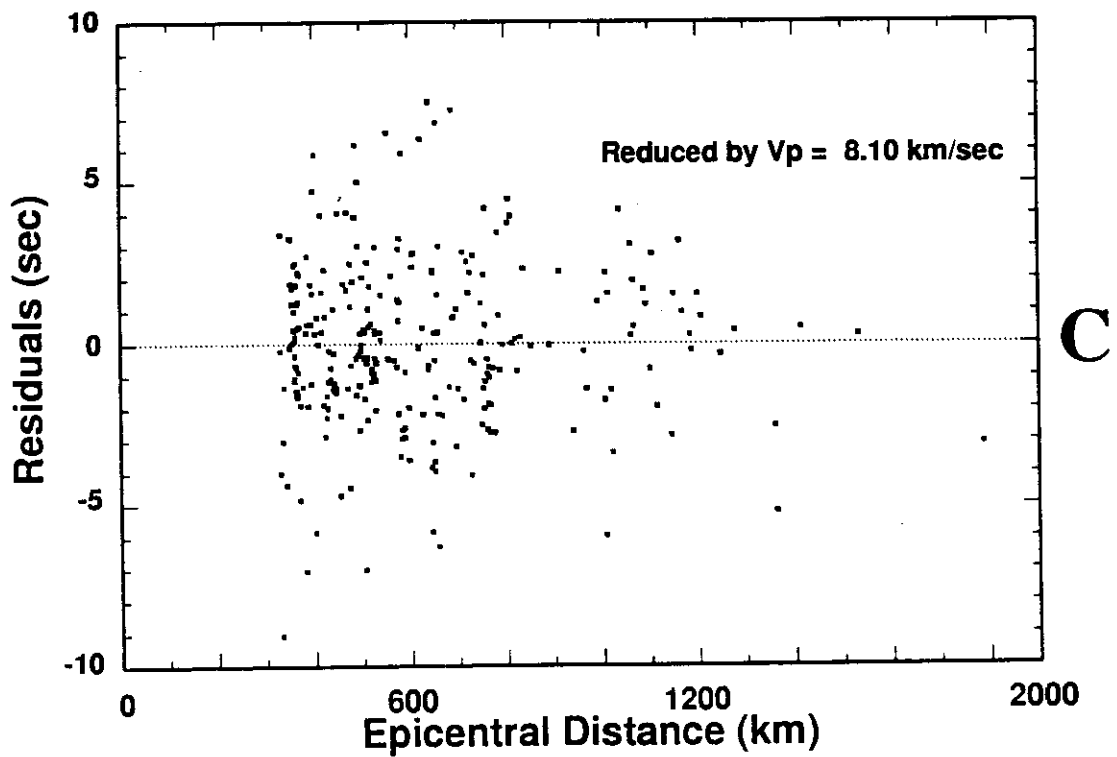
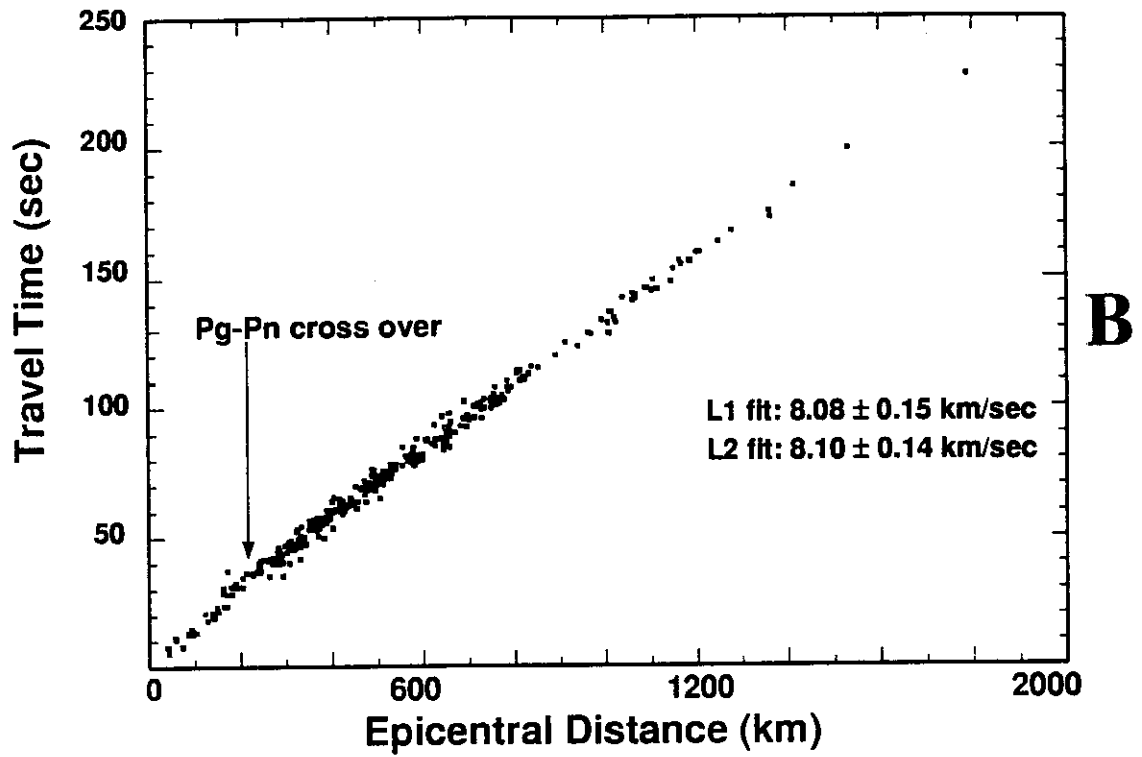


(Figure 2: McNamara et al., 1994)

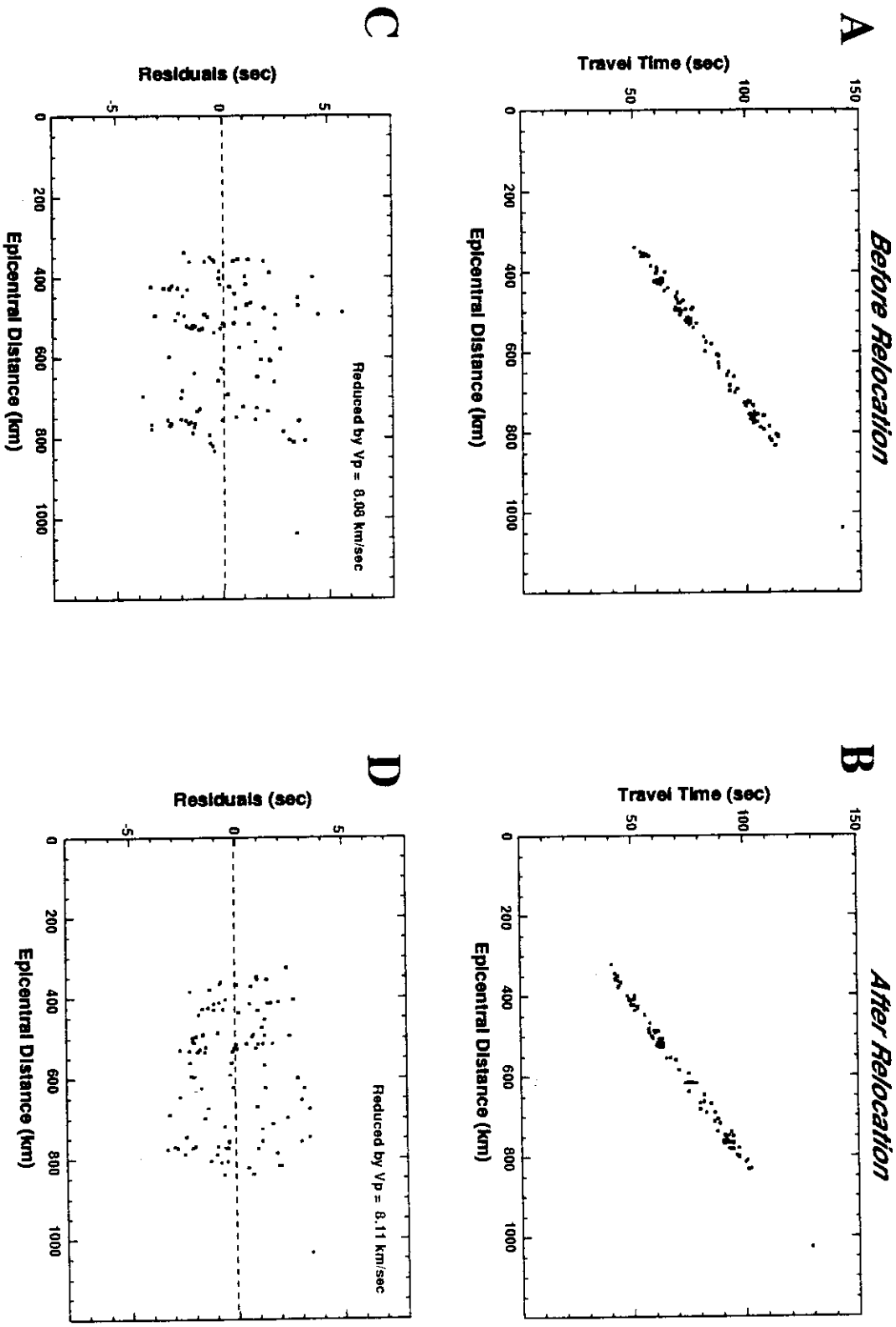
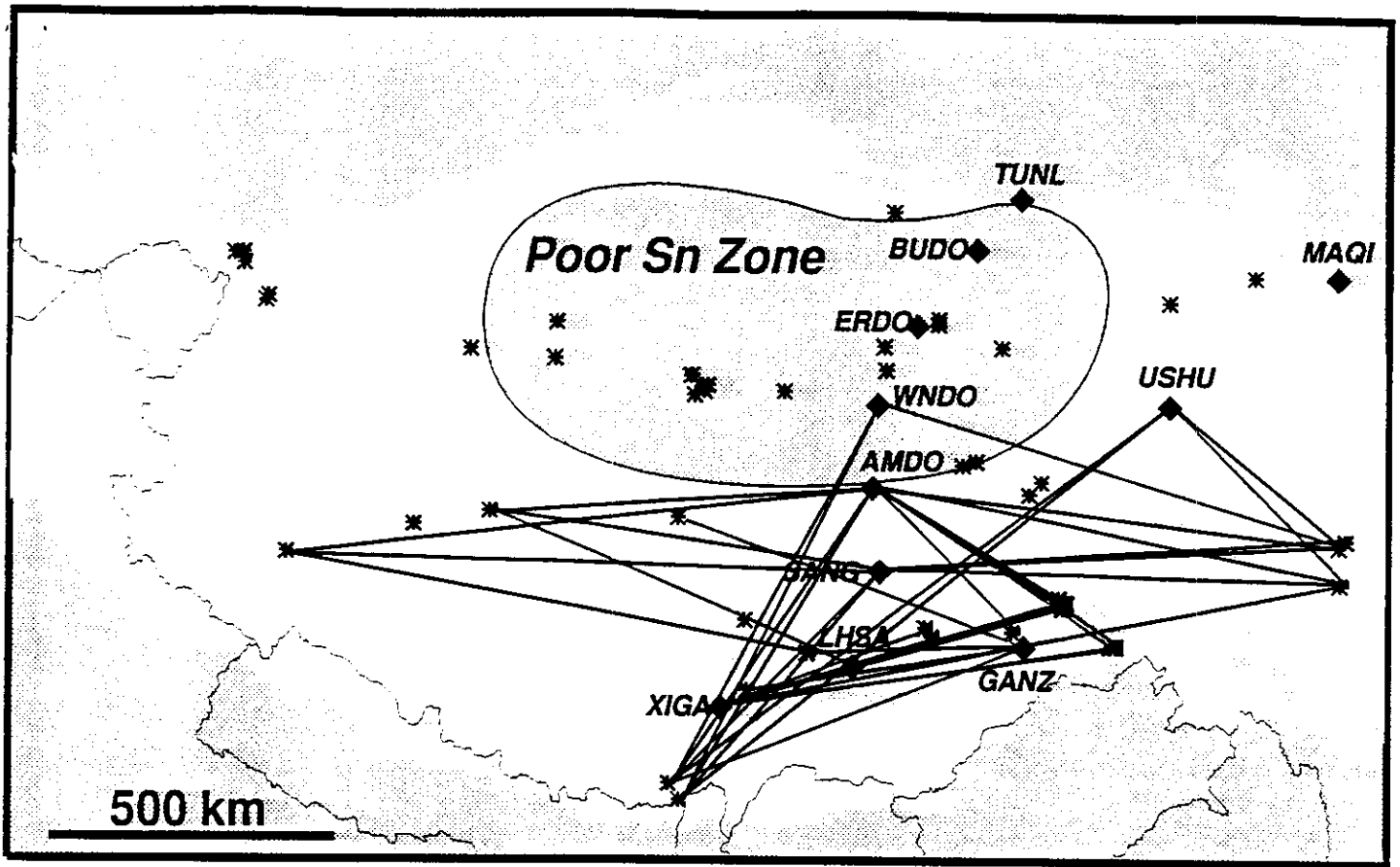
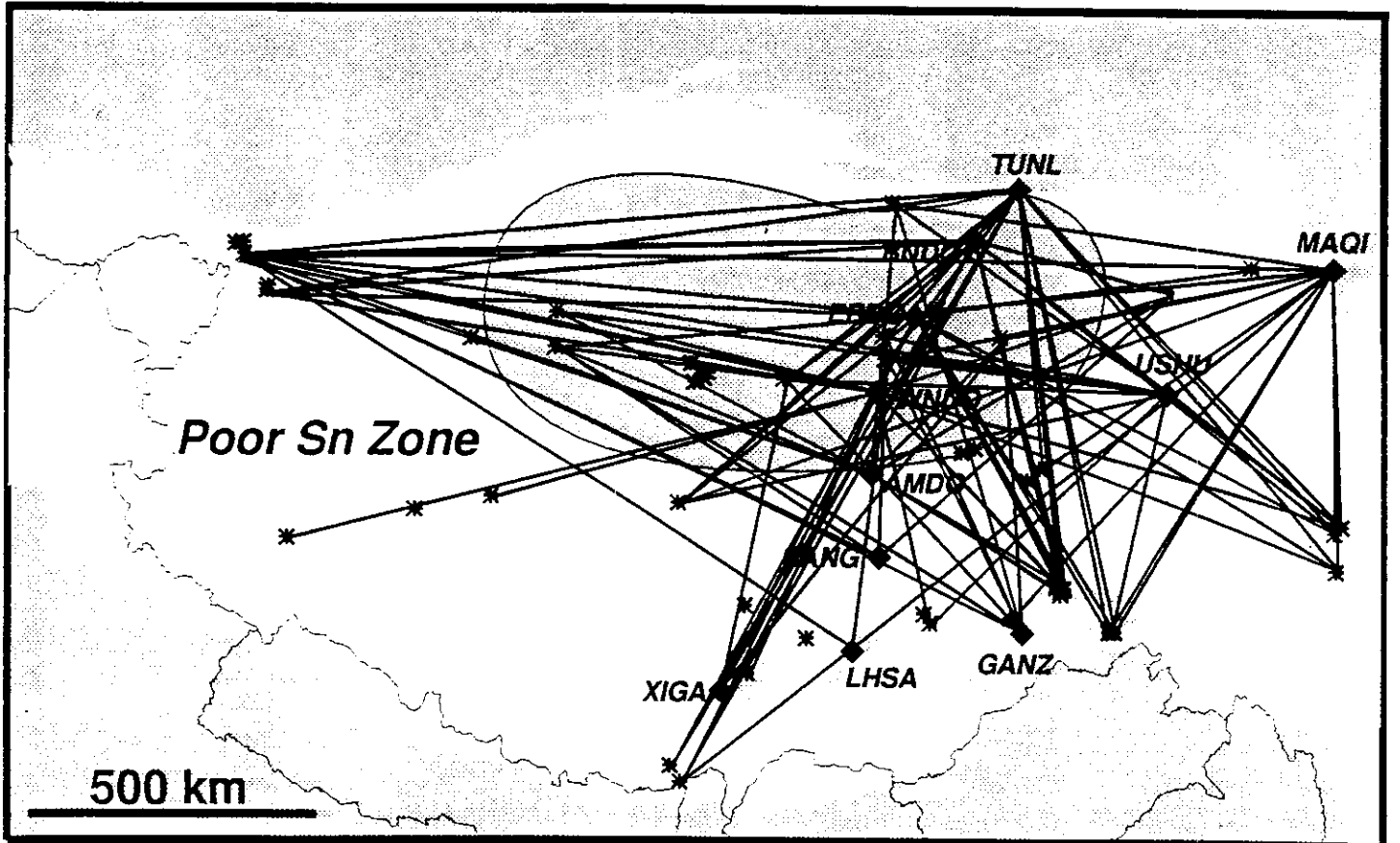


Figure 3: McNamara et al., 1994)

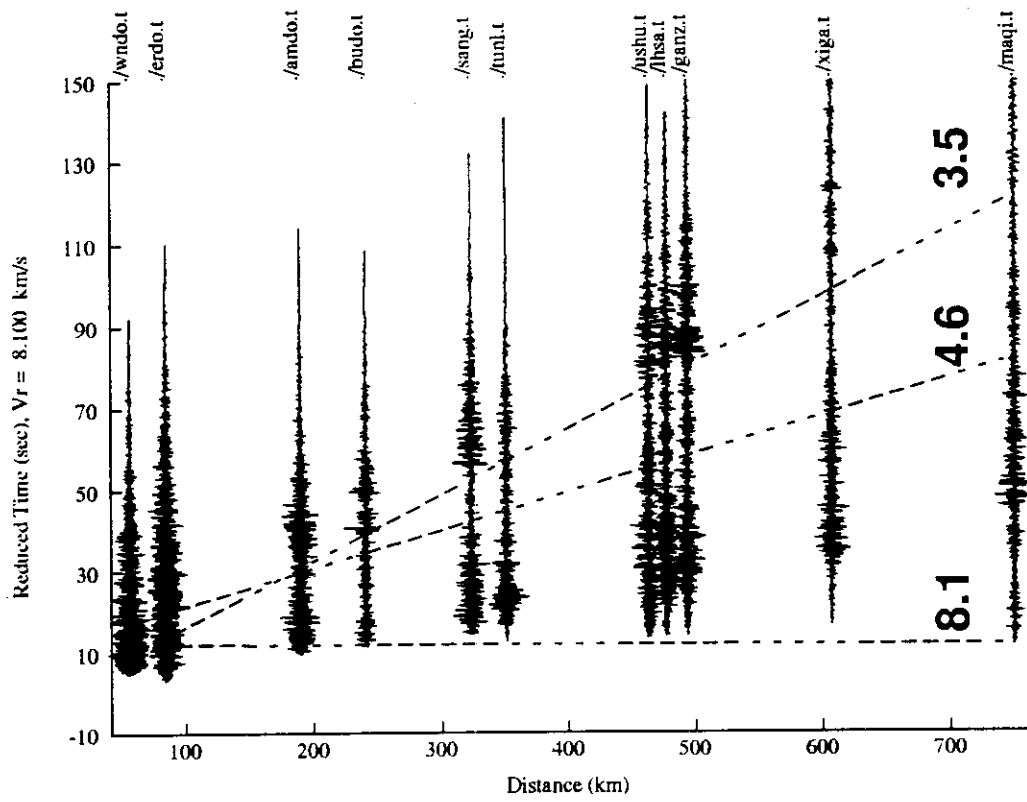


B: Paths with no observable Sn



(Figure 4: McNamara et al., 1994)

91.222.20.21.24 Tangential (1-5Hz) 33.910 N 92.158 E



91.222.20.21.24 Radial (1-5Hz) 33.910 N 92.158 E

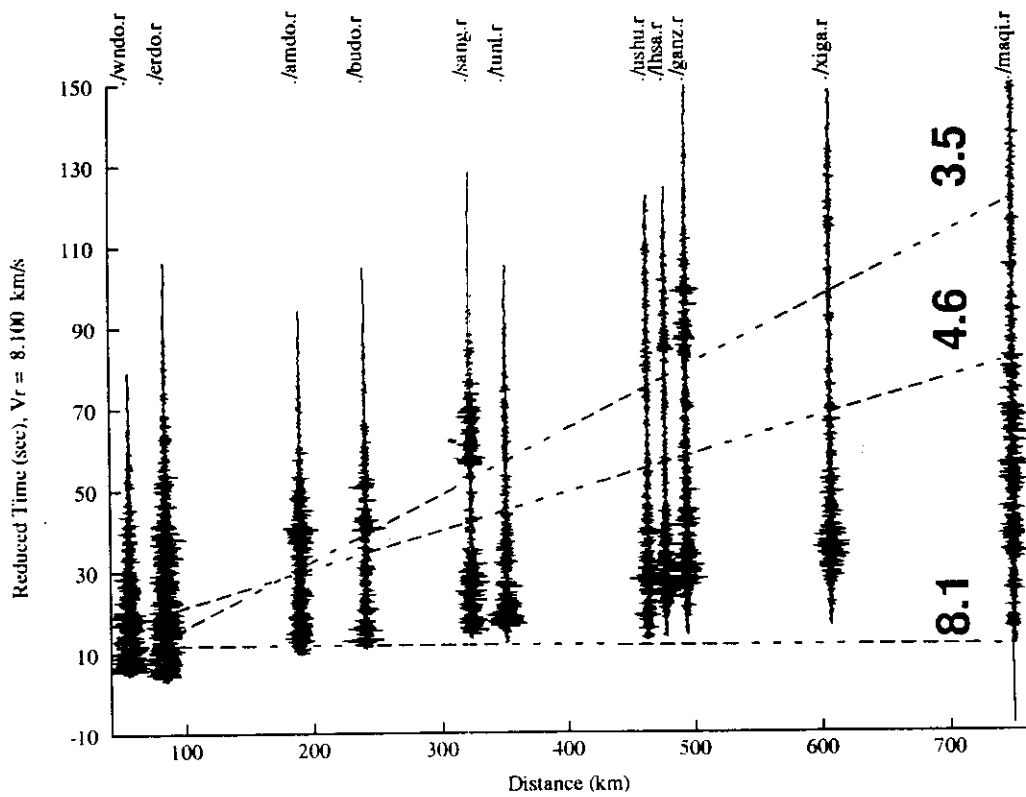


(Figure 5: McNamara et al., 1994)

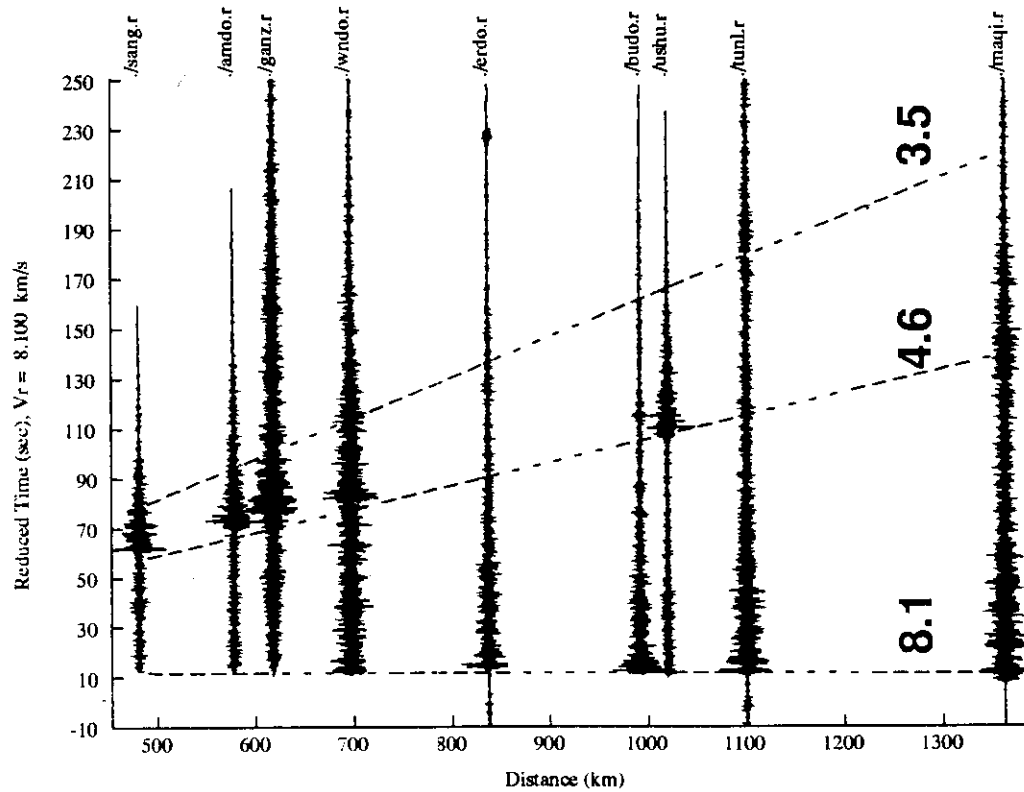
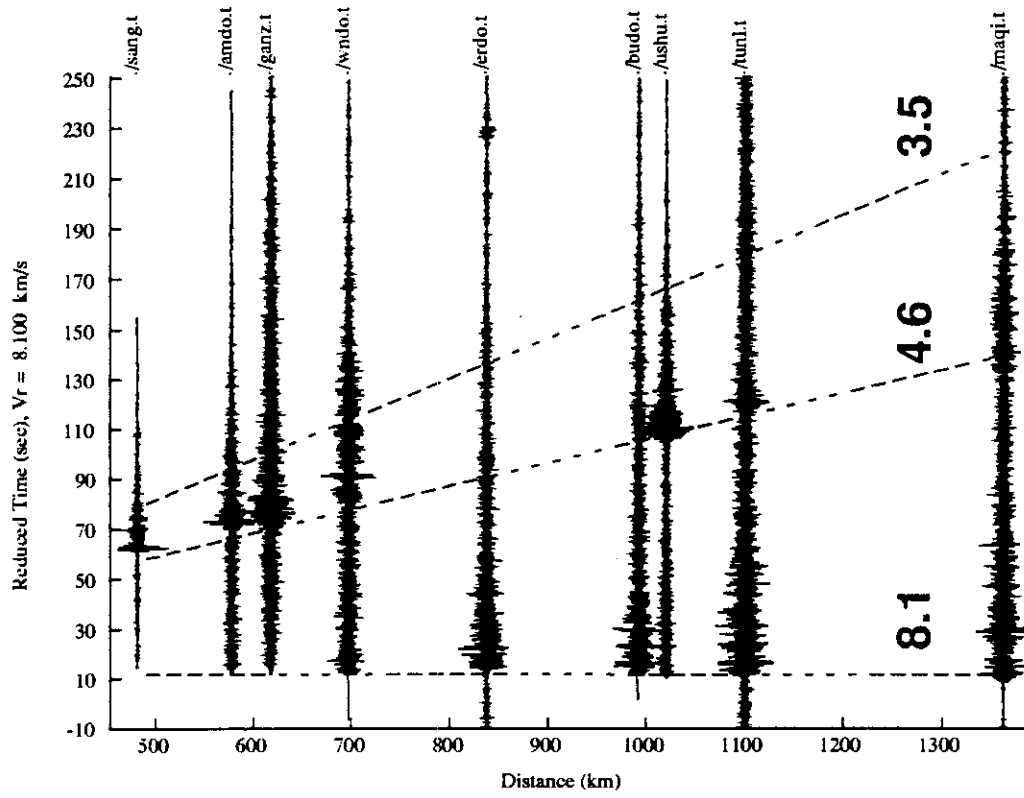
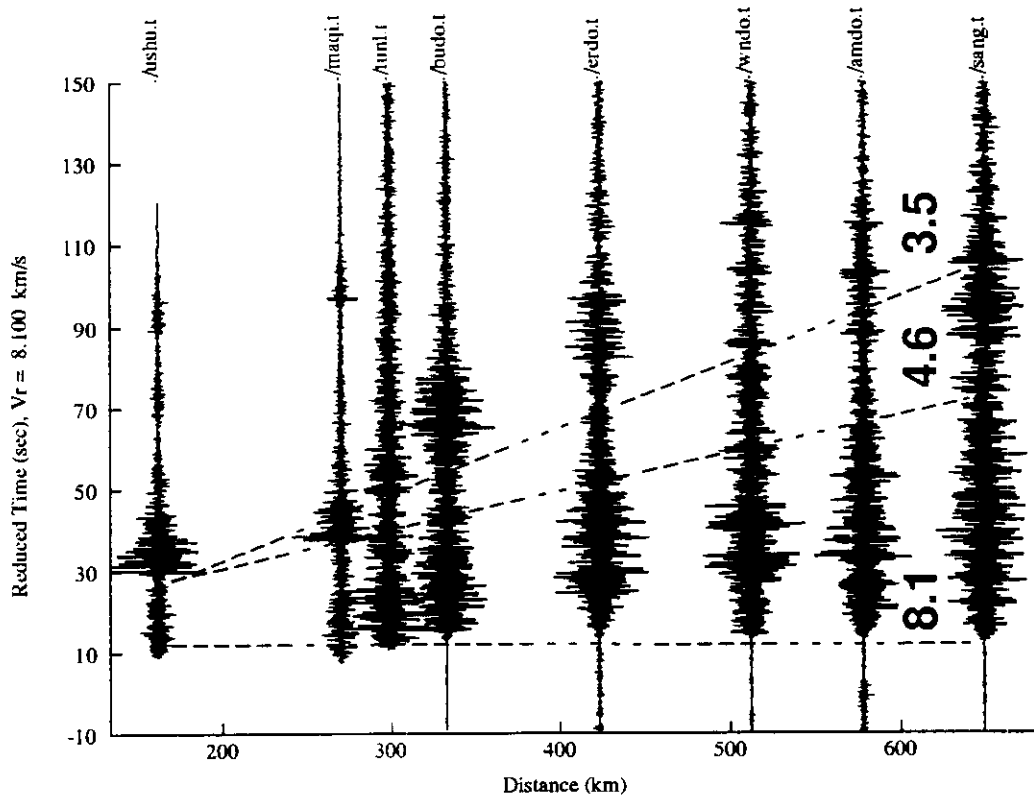


(Figure 6: McNamara et al., 1994)

91.242.14.30.58 Tangential (1-5Hz) 34.449 N 97.309 E



91.242.14.30.58 Radial (1-5Hz) 34.449 N 97.309 E

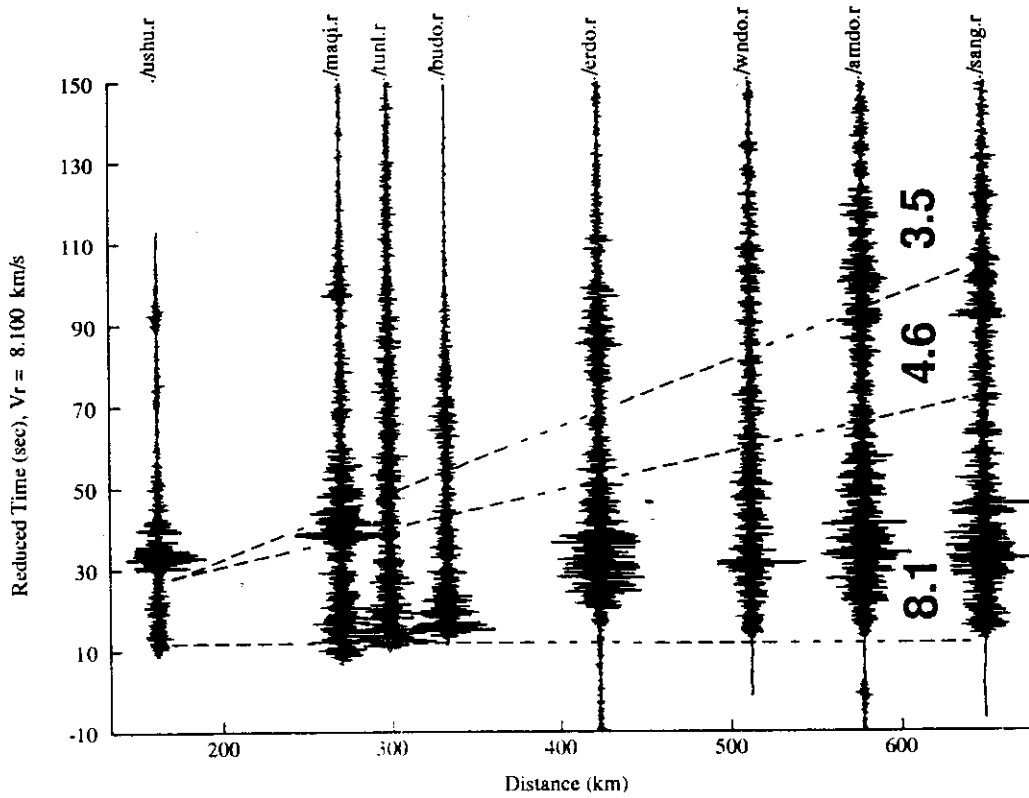
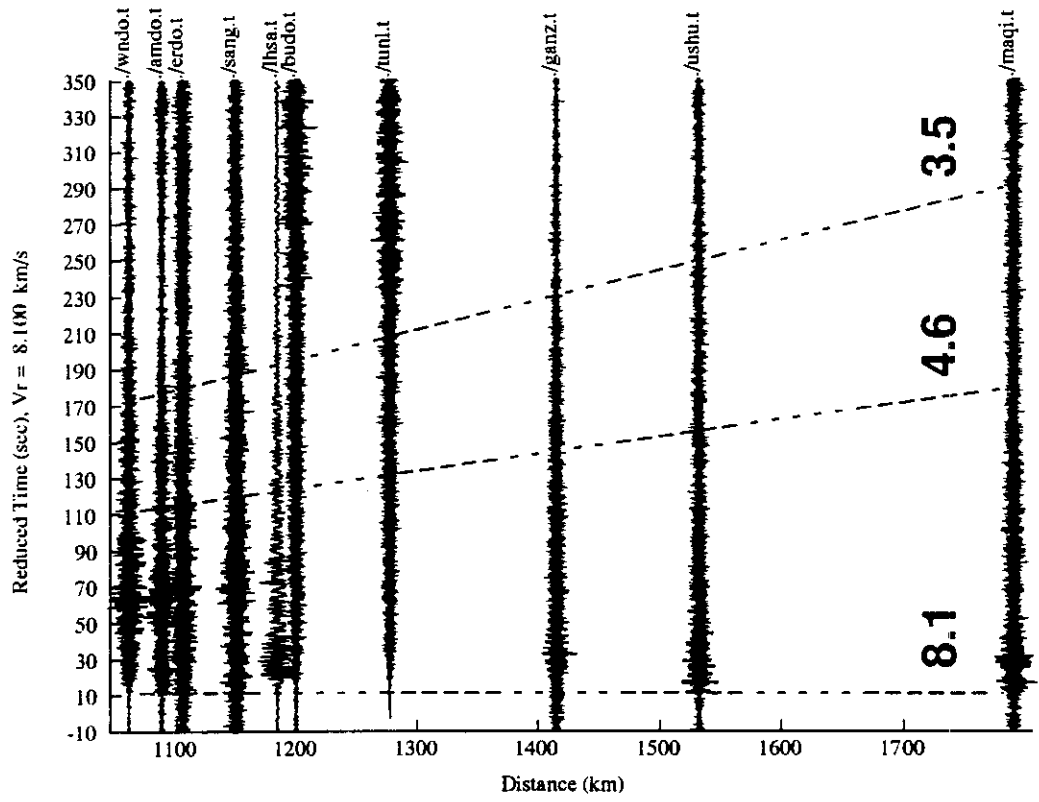


(Figure 7: McNamara et al., 1994)

92.096.07.47.27 Tangential (1-5Hz) 35.696 N 80.661 E



92.096.07.47.27 Radial (1-5Hz) 35.696 N 80.661 E

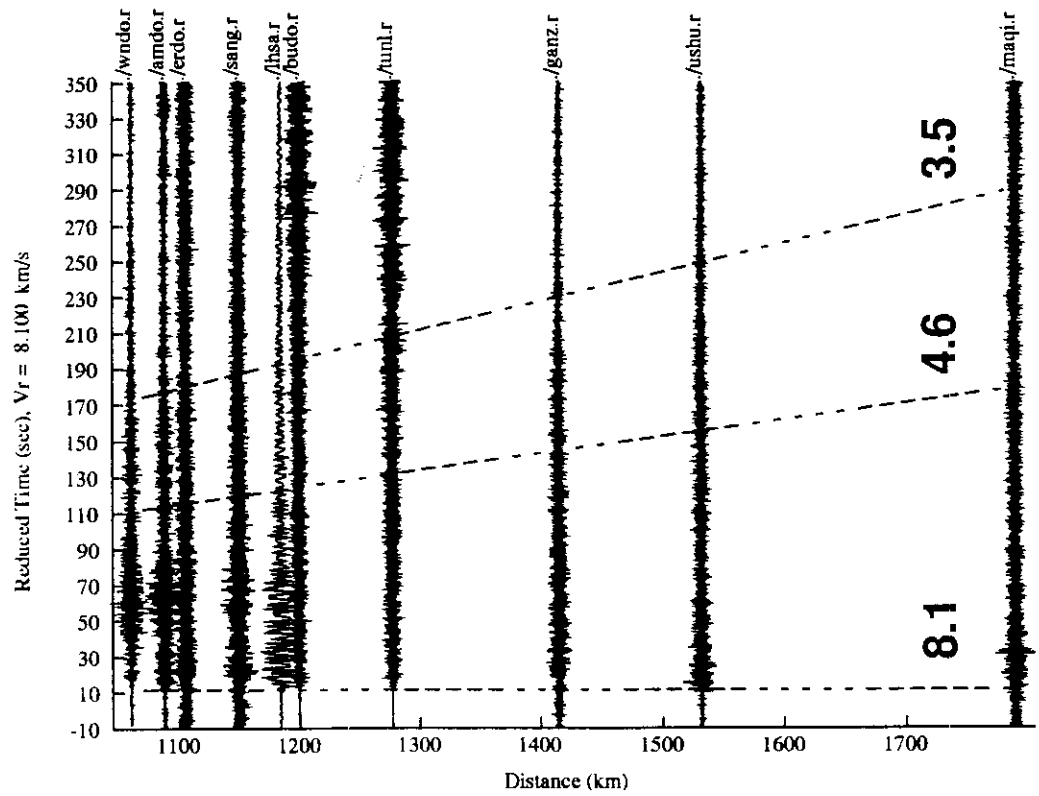


(Figure 8: McNamara et al., 1994)

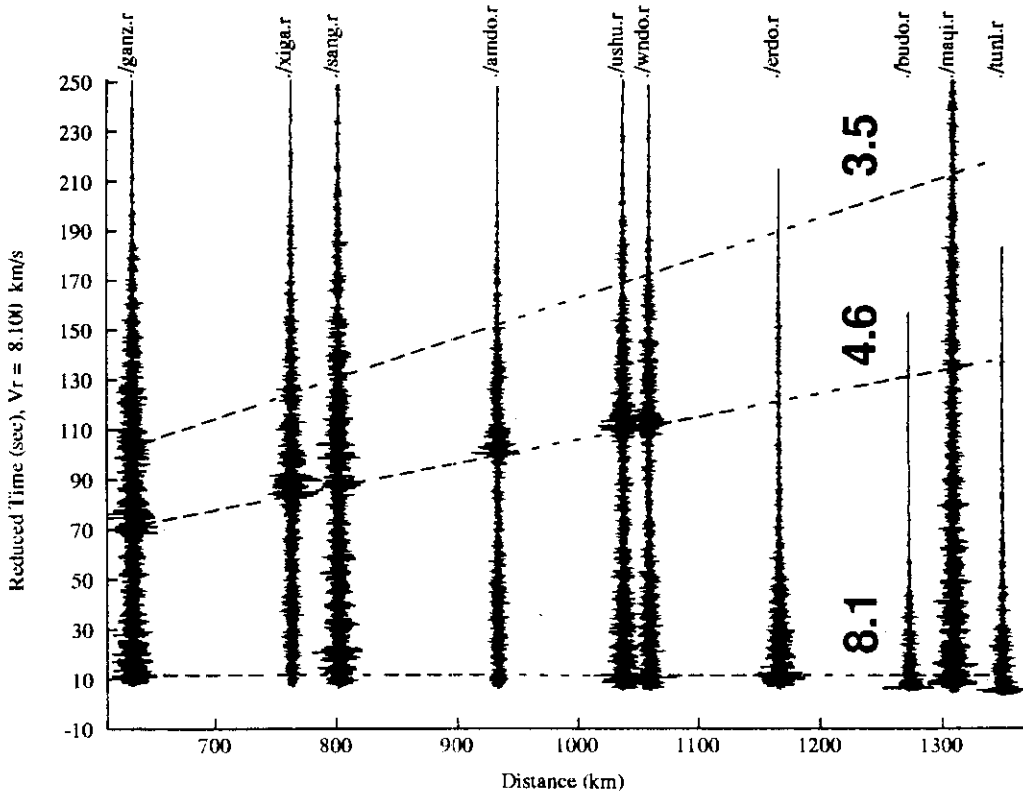
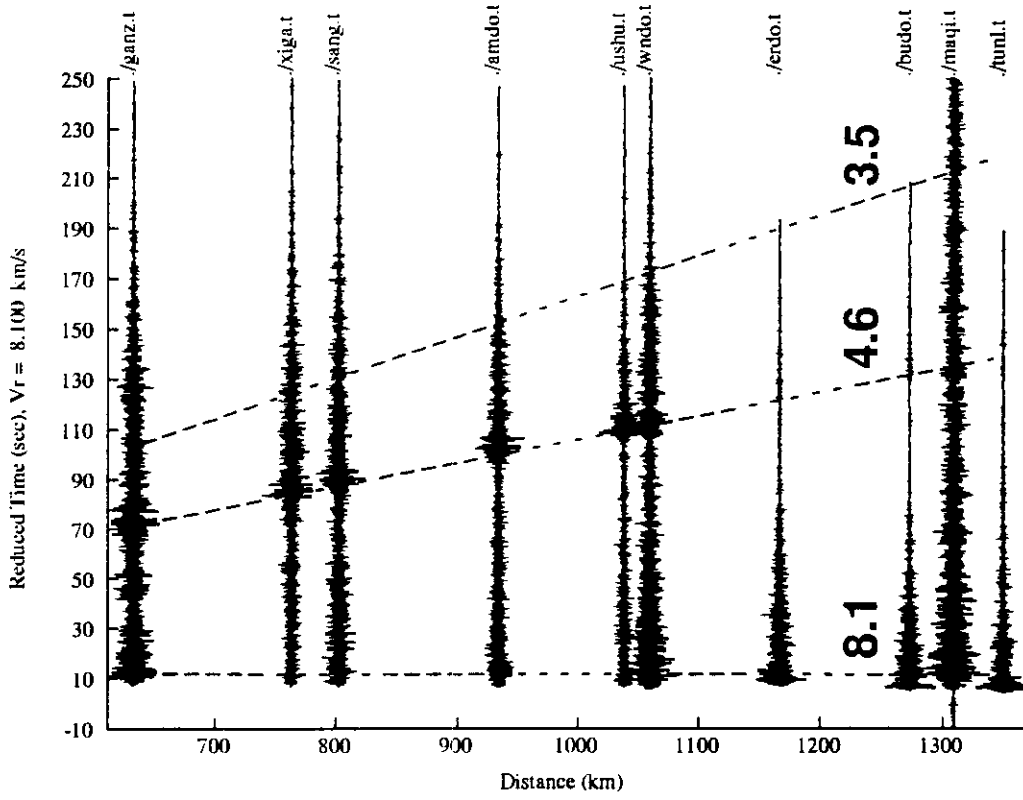


(Figure 9: McNamara et al., 1994)

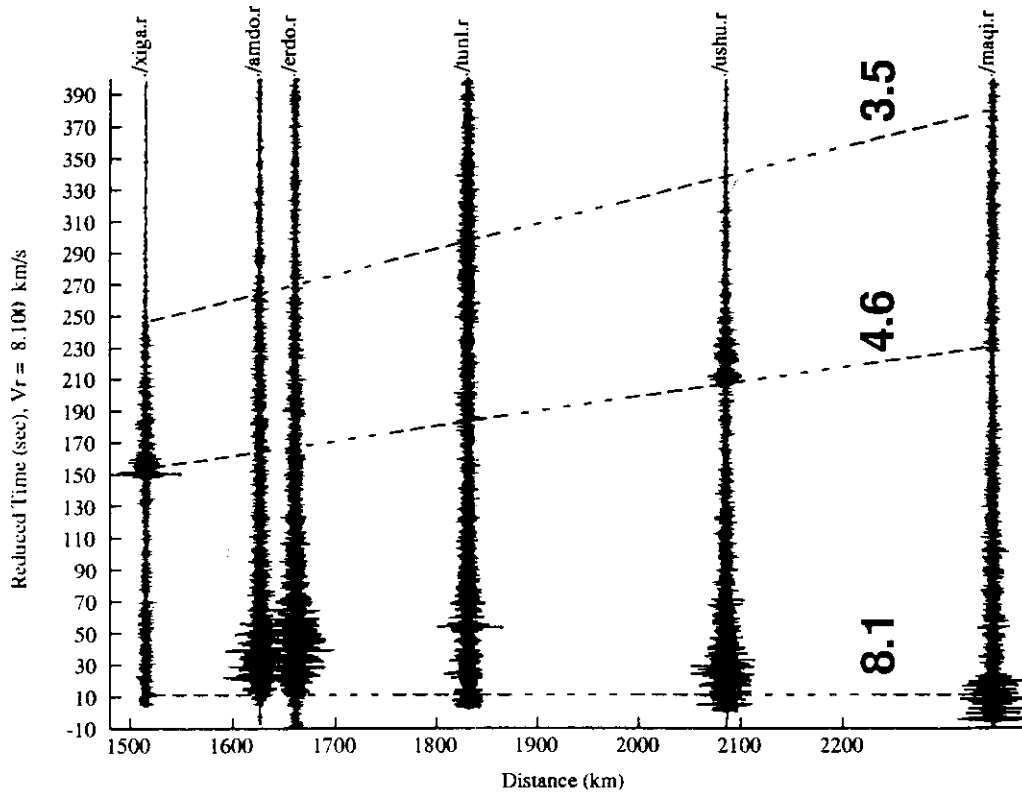
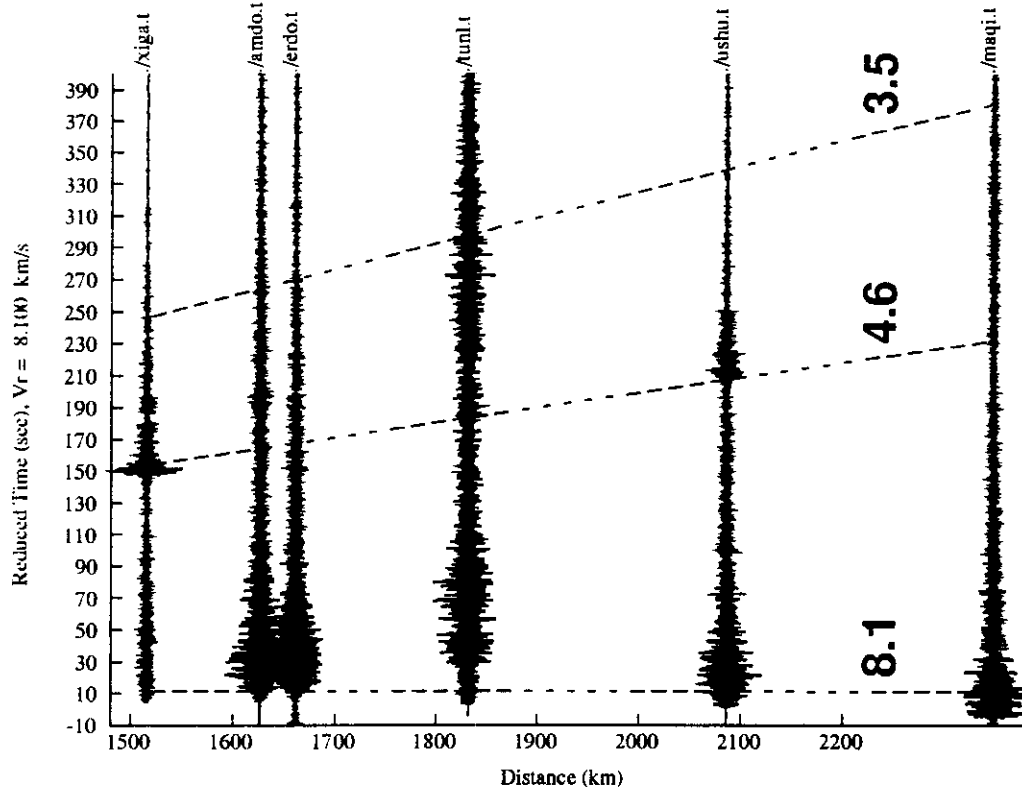
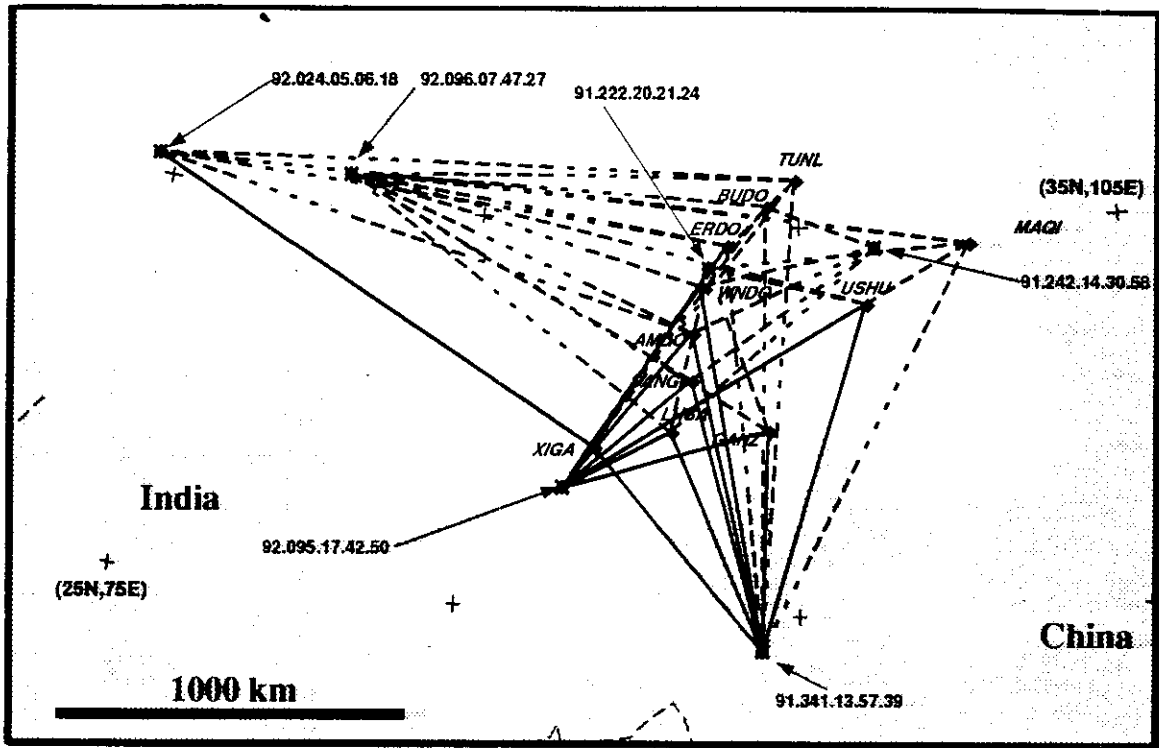


(Figure 10: McNamara et al., 1994)

A



B

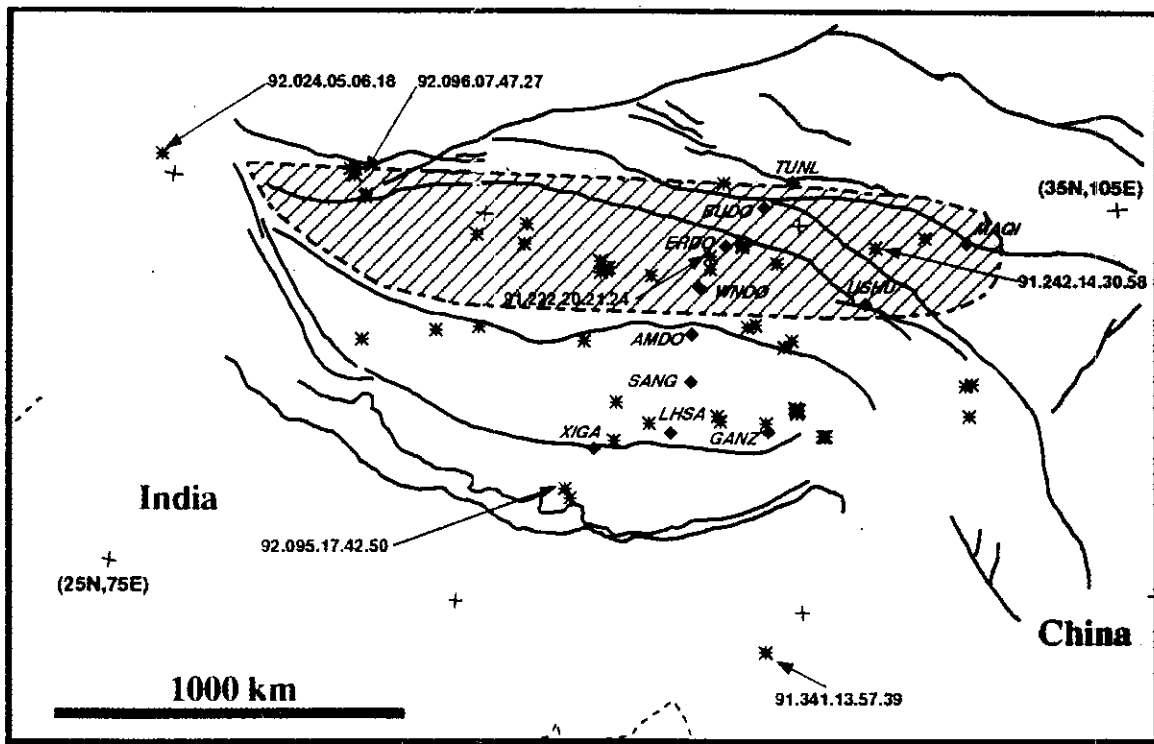


(Figure 11: McNamara et al., 1994)